Influence of the electronic structure on the transport properties of some iron pnictides

F. Rullier-Albenque

C. R. Physique 17 (2016) 164–187

Contents lists available at ScienceDirect

Comptes Rendus Physique

www.sciencedirect.com

Iron-based superconductors / Supraconducteurs à base de fer

Influence of the electronic structure on the transport properties of some iron pnictides

Influence de la structure électronique sur les propriétés de transport de quelques pnictures à base de fer

Florence Rullier-Albenque

Service de l'État Condensé, IRAMIS, CEA, CNRS UMR 2464, Université Paris-Saclay, Orme des Merisiers, CEA Saclay, 91191 Gif-sur-Yvette cedex, France

ARTICLE INFO

Article history:
Available online 11 November 2015

Keywords:
Iron pnictides
Transport properties
122 family
111 LiFeAs compound

Mots-clés :
Pnictures de fer
Propriétés de transport
Famille des 122
Compose 111 LiFeAs

ABSTRACT

An important feature of the iron-based pnictides is their multi-band electronic structure with both electron and hole bands at the Fermi level. The size of these pockets can be changed by different types of substitution, resulting in a variety of original magnetic and electronic properties. The contributions of both types of carriers will thus have important consequences on the evolution of the transport properties versus temperature and doping. It has been pointed out that Hund's rule interaction plays a prominent role in the physics of these compounds by allowing a strong orbital differentiation between the 3d Fe orbitals. As a result, a description in terms of more or less correlated electrons was proposed and may have important consequences on the scattering lifetimes of the different carriers. Finally, the presence of very flat bands at the Fermi level may induce a semiconductor-like behavior, with a change in carrier concentration with temperature. In this paper, we will review the evolution of transport properties with chemical doping/substitution in iron pnictides. We will more particularly focus on the 122 family ($Ba(Sr,Ca)Fe_2As_2$) and the 111 LiFeAs compound for which sizeable single crystals required for transport measurements are available. The combined resistivity, Hall effect and magnetoresistance data will be analyzed in association with electronic structure calculations, angle-resolved photoemission measurements and quantum oscillations. In spite of the strong interplay between antiferromagnetism and superconductivity in most part of their phase diagram, direct signatures of spin fluctuations are difficult to identify in the transport properties of iron pnictides. We will show that measurements of the longitudinal magnetoresistance provide a powerful tool for studying the coupling between the charge carriers and the spin degrees of freedom.

RÉSUMÉ

Une caractéristique importante des pnictures à base de fer est leur structure électronique « multi-bandes » présentant à la fois des bandes d'électrons et de trous au niveau de Fermi. La taille de ces poches peut être changée par différents types de substitution, ce qui entraine une grande diversité de propriétés magnétiques et électroniques originales. On

E-mail address: florence.albenque-rullier@cea.fr.

http://dx.doi.org/10.1016/j.crhy.2015.10.007
1631-0705/

s'attend également à ce que la contribution des deux types de porteurs ait une importance considérable sur les propriétés de transport en fonction de la température et du dopage. Il a été également souligné que l'interaction de Hund joue un rôle prépondérant dans la physique de ces composés en permettant une forte différenciation entre les orbitales 3d du Fe. En conséquence, une description en termes d'électrons plus ou moins corrélés a été proposée, ce qui pourrait avoir d'importantes conséquences sur les temps de diffusion des différents porteurs de charge. Enfin la présence de bandes très plates au niveau de Fermi est susceptible d'induire un comportement de type « semiconducteur », avec un changement de la concentration des porteurs de charge avec la température. Dans ce papier, nous allons passer en revue l'évolution des propriétés de transport avec la substitution ou le dopage chimique dans les pnictures de fer. Nous allons plus particulièrement nous intéresser à la famille des composés 122 (Ba(Sr,Ca)Fe2As2) et du composé 111 LiFeAs pour lesquels des monocristaux de taille adaptée à la mesure des propriétés de transport sont disponibles. Les données combinées de résistivité, effet Hall et magnétorésistance seront analysées en association avec les calculs de structure électronique, les mesures de photoémission résolues en angle et oscillations quantiques. En dépit de la forte interaction entre antiferromagnétisme et supraconductivité dans la plus grande partie de leurs diagrammes de phase, la signature des fluctuations de spin n'apparait pas directement dans les propriétés de transport des pnictures de fer. Nous montrerons que la mesure de la magnétorésistance longitudinale fournit une sonde intéressante pour étudier le couplage entre les porteurs de charge et les degrés de liberté de spin.

1. Introduction

Despite the strong similarities between the phase diagrams of high-T_c cuprates and iron-based superconductors (FeSC), a crucial difference comes from the fact that the former are single-band materials while all the d orbitals of iron participate in the electronic structure at the Fermi level for FeSC. This usually results for all the FeSCs in five Fermi surface sheets: three hole pockets around the center of the Fe_2As_2 Brillouin zone and two electron pockets around the corners as predicted by band structure calculations and evidenced by angle resolved photoemission spectroscopy (ARPES) [1–3].

This rather complex multi-band electronic structure is one of the key ingredient to understand the physical properties of the FeSCs and has important consequences on the superconducting and normal state properties of these compounds. In the undoped compounds the spin density wave (SDW) ordering below T_N is widely attributed to the nesting between electron and hole quasi-cylindrical bands, which leads to a reconstruction of the Fermi surface and a strongly peaked spin susceptibility at the antiferromagnetic (AF) wave vector Q_{AF}. It was argued very early that SC could be also mediated by spin fluctuations at the same wave vector, resulting in an extended s-wave pairing with sign change of the order parameter between electron and hole sheets [4,5].

The transport properties are also expected to be very sensitive to any modifications of the Fermi pockets as a function of temperature, doping or pressure. As a matter of fact, resistivity measurements provide the simplest experimental way to follow the evolution of the physical properties. This is for instance illustrated in Fig. 1 where the temperature resistivity curves are reported as a function of Co substitution in the $Ba(Fe_{1-x}Co_x)_2As_2$ compound [6]. Starting from the parent compound $BaFe_2As_2$ where the magnetostructural transition is evidenced by the sharp drop of the resistivity at $T_S = T_N$, one can then easily follow the decrease in T_S and T_N and the appearance of superconductivity with Co substitution, allowing one to construct the phase diagram. We can also notice that a marked change in the evolution of $\rho(T)$ occurs at about $x = 0.03$, for which superconductivity appears.

It appears much more complicated to understand the temperature dependence of the resistivity and its evolution with Co substitution. For instance it is striking to see that the high-T parts of the resistivity shift downwards parallel each other for weak Co substitution (dashed curves in Fig. 1a). This clearly cannot be understood within a one single band picture. Indeed in that case, using a simple Drude formula and Matthiessen's rule, the resistivity ρ writes as:

$$\rho = m^*/ne^2\tau = m^*/ne^2(1/\tau_e + 1/\tau_{in}(T)) \quad (1)$$

with m^*, n and τ_e and τ_{in}, the effective mass, number of carriers and elastic and inelastic scattering time of the carriers respectively. Knowing that Co electron dopes the system, one would expect changes of the slope of the resistivity curves with Co substitution, contrary to what is observed.

Thus the transport properties of FeSCs will depend in a non-trivial manner on the number of carriers in the different Fermi pockets and their respective intra- and inter-band scatterings. The scope of this paper is to review the evolution of their transport properties – resistivity, Hall effect and magnetoresistance – in relationship with what is known on their electronic structure either theoretically by band structure calculations or experimentally by ARPES or quantum oscillations studies. We will restrict ourselves to the iron pnictides and more particularly to those for which sizeable single crystals can be synthesized, a prerequisite to get good measurements of transport properties. Most of the paper will be thus devoted

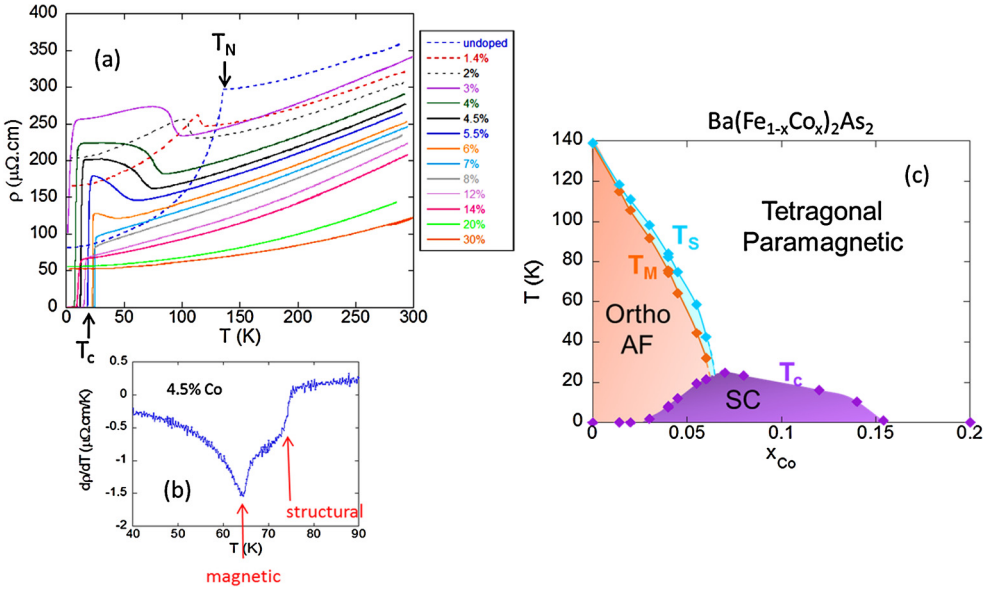

Fig. 1. (a) Resistivity curves of the 122-compound $Ba(Fe_{1-x}Co_x)_2As_2$ for different Co concentrations (from [6]). The evolution of the superconducting transitions can be easily determined. Anomalies of the resistivity allow one to determine both the structural and the magnetic transition temperatures by looking at the temperature derivative of resistivity as shown in (b) and to build up the phase diagram of this compound as a function of Co substitution (c).

to the very rich 122 $BaFe_2As_2$ family which has been the most extensively studied system since superconductivity can be obtained by very different routes – electron or hole doping, isovalent substitution and pressure. Another compound that is particularly interesting is the 111 compound LiFeAs since it is the only nearly stoichiometric compound, together with NaFeAs and KFe_2As_2, which is superconducting without any substitution. Moreover, due to the neutral surface of LiFeAs after cleaving, one does not expect any influence of the surface on the electronic states. Therefore the data of surface sensitive probes such as angle resolved photoemission spectroscopy (ARPES) are very well representative of the bulk properties [7].

2. 122 compounds

Among the 122 system, $BaFe_2As_2$ appears as the prototypical iron pnictide compound as superconductivity can be induced either by substitution on the iron site (electron doping by Co or Ni [8–10]; isovalent substitution by Ru [11,12]), substitution on the Ba site (hole doping by potassium substitution [13]) or substitution on the As site (isovalent phosphorus substitution [14–16]) (more references can be found in the paper of Martinelli et al. [18]). This provides an exceptional playground to study the different modifications of the electronic structure and their consequences on the transport properties. Albeit less studied, all these substitutions are also possible in the $SrFe_2As_2$ family and display a lot of similarities with the behavior observed in the $BaFe_2As_2$ family.

However substitution effects in the $CaFe_2As_2$ family appear quite different, probably related to the existence of the collapsed tetragonal phase observed in the pure $CaFe_2As_2$ under pressure. Although onsets of superconducting transition temperatures as high as 47 K, the maximum so far among the 122 family, were observed by aliovalent substitution into the alcaline earth site of $CaFe_2As_2$ single crystals [17], there is some doubt about the bulk nature of this superconductivity. Moreover the morphology of these crystals appear to be strongly dependent on the annealing conditions and not very reproducible [19]

2.1. Parent compounds and electron doping on iron site by transition metal substitution

Iron substitutions by atoms situated at the right of iron in the periodic table are expected to electron dope the system. This was clearly evidenced by ARPES measurements [22,24] which showed that the areas of the hole bands decrease and those of the electron bands increase upon Co or Ni substitution, contrary to some theoretical proposals [25]. Moreover as shown in Fig. 2, the phase diagrams for these two substitutions match with each other if they are plotted as a function of electron doping, showing unambiguously that each Co (Ni) atom adds one (two) electron(s) to the bands. The same observation was found for Rh and Pd substitutions [26].

2.1.1. Transport in the high-temperature paramagnetic phase

Resistivity As already pointed out above, the effect of electron doping does not appear on the resistivity curves straightforwardly. First let us note that the iron pnictides were sometimes qualified as “bad metals” due to the fact that their

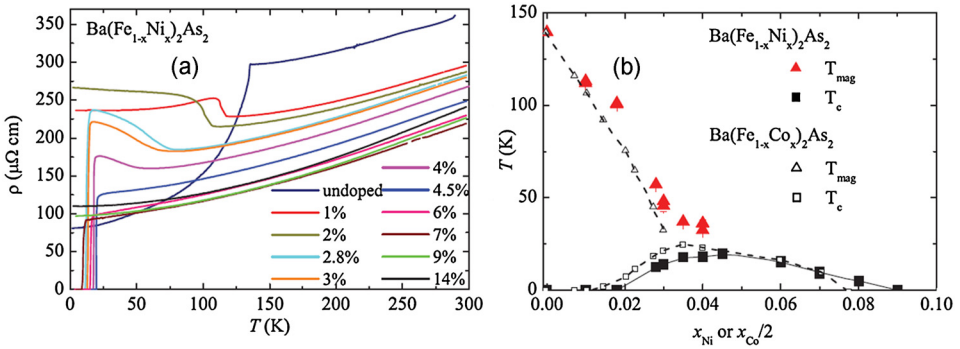

Fig. 2. (a) Resistivity curves of the 122-compound $Ba(Fe_{1-x}Ni_x)_2As_2$ for different Ni concentrations (from [20]). The evolution of the $\rho(T)$ curves with Ni substitution is very similar to that obtained with Co substitution see Fig. 1. (b) Phase diagram indicating T_{mag} and T_c for the two families. A close matching is obtained by plotting the data versus x_{Ni} and $x_{Co}/2$.

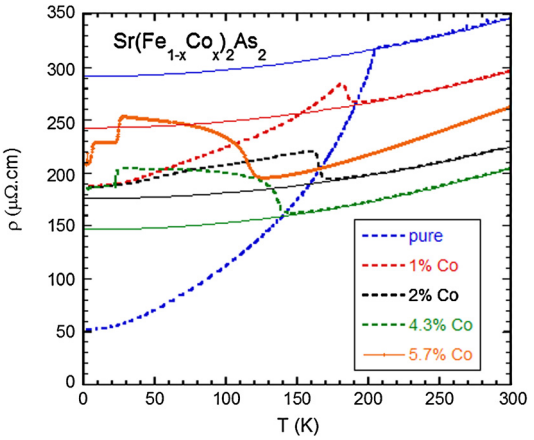

Fig. 3. Temperature resistivity curves of $Sr(Fe_{1-x}Co_x)_2As_2$ for low Co dopings. The high-T paramagnetic parts are well fitted by $A + BT^2$ (full lines) with A decreasing with Co contents and B remaining nearly constant. From [31].

resistivities are rather high and do not saturate at high temperature [27,28]. However, the observation of a Drude like component at low frequencies in the optical conductivity of iron pnictides reveals the presence of itinerant electrons more or less correlated depending on the system. Moreover, in the case of $BaFe_2As_2$, the fact that the $\rho(T)$ curve can be well fitted by $A + BT^2$ in the high-T paramagnetic phase, as noticed recently in Ref. [30], indicates conventional Fermi liquid behavior with considerable elastic scattering, A being much larger than BT^2. However it is worth mentioning here that ARPES measurements have evidenced a strong increase of the number of electrons with temperature in this temperature range [29] (see Fig. 6 below), which indicates that some care should be taken to extract the genuine T dependence of the scattering rates of the carriers from resistivity measurements.

In any case, it is very puzzling to see that the effect of tiny substitution by Co (see Fig. 1a) or Ni (see Fig. 2a) is to decrease A while maintaining BT^2 nearly constant. The same behavior is exemplified in the case of $Sr(Fe_{1-x}Co_x)_2As_2$ as reported in Fig. 3 [31]. These observations seem to indicate that the initial introduction of Co or Ni in the FeAs slabs does not change the number of carriers but decrease the residual impurity scattering. This is quite opposite to what is expected, since these impurities located in the Fe planes will be strong scatterers especially for electrons in narrow bands. Clearly more theoretical work is needed to explain this first evolution of the transport properties.

Upon further substitutions by Co or Ni an increase in the slope of the paramagnetic part of $\rho(T)$ is observed at high temperature for all the compounds. As seen in Fig. 1 or Fig. 2, this change of behavior is concomitant with the apparition of superconductivity. Moreover this is also associated with a drastic modification of the electronic structure in the reconstructed magnetic phase as evidenced by Hall effect, thermoelectric power and ARPES measurements. These different effects will be described in the next paragraphs.

Hall effect Hall effect measurements allow one to get more insight into the evolution of the transport properties in the paramagnetic high-T phase. The Hall resistivity is always linear with magnetic field allowing one to determine the Hall coefficient R_H unambiguously. This is no longer true in the magnetic phase where a saturation with magnetic field is observed upon decreasing the temperature (see below) [6,32]. The data for the Hall coefficient R_H are presented in Fig. 4a for a set of Co dopings in $BaFe_2As_2$. The strong increase in the magnitude of R_H is correlated to the reconstruction of the

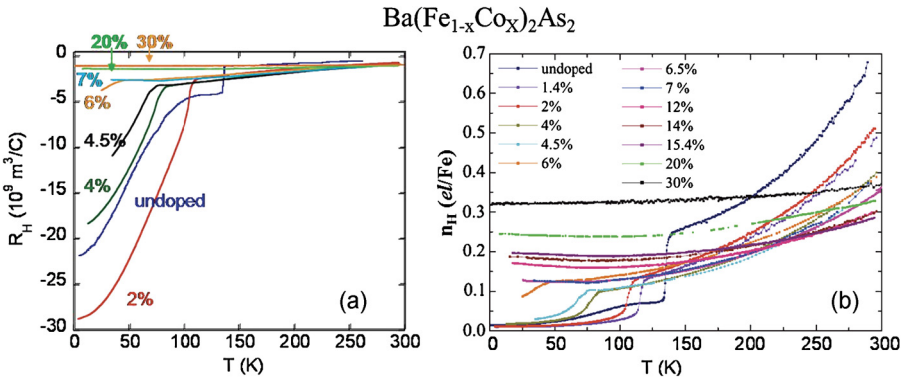

Fig. 4. (a) Temperature dependence of the Hall coefficient for a series of $Ba(Fe_{1-x}Co_x)_2As_2$ crystals. The drop of R_H signals the reconstruction of the Fermi surface at T_N. To see more clearly the evolution in the paramagnetic phase, the Hall number $|n_H|$ is plotted in (b) versus temperature. Here, $n_H(e/\mathrm{Fe}) = 0.32/R_H x(10^{-9}\ \mathrm{m}^3/\mathrm{C})$. From [6].

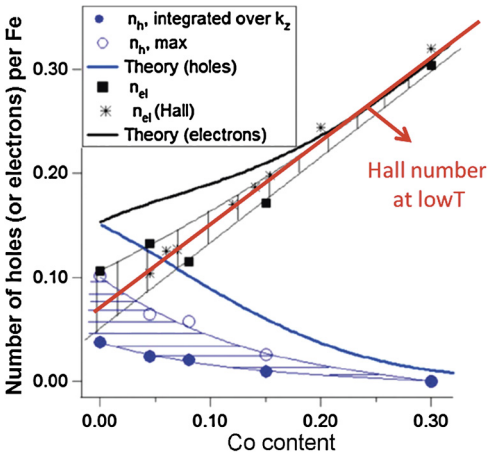

Fig. 5. Number of holes (open blue circles) and electrons (black squares) extracted from ARPES measurements on $Ba(Fe_{1-x}Co_x)_2As_2$ single crystals from the same batches as used for resistivity measurements. Solid blue circles indicate the number of holes after correction taking into account the three dimensional geometry of the hole pockets. Black stars are the low T data for $|n_H|$ reported in Fig. 4b. Hatched areas indicate likely values for the number of holes and electrons, including possible experimental errors. Thick black and blue solid lines are prediction of LDA calculations for the evolution of number of holes and electrons [32] reproduced from Ref. [25].

Fermi surface at the magnetic transitions. In order to better visualize the behavior of R_H in the paramagnetic phases and for large x, we have plotted in Fig. 4b the variations of the Hall number $n_H = 1/(eR_H)$.

The strong variation of $|n_H|$ with temperature indicates that several bands contribute to the transport. Moreover the negative sign of R_H points out that electrons give the dominant contribution to the charge transport at all T whatever x. Assuming a simple two band model as a starting point, one could write:

$$\sigma = 1/\rho = \sigma_h + \sigma_e \tag{2}$$

$$eR_H = \frac{1}{n_H} = \frac{\sigma_h^2}{n_h(\sigma_e + \sigma_h)^2} - \frac{\sigma_e^2}{n_e(\sigma_e + \sigma_h)^2} \tag{3}$$

where n_e (n_h) are the concentration of electrons (holes) usually taken as T independent in a metallic state. One should note that charge conservation implies:

$$n_e = n_h + x \tag{4}$$

with the usual assumption that Co gives one electron to these bands. As we have only three relations for $n_e, n_h, \sigma_e, \sigma_h$, this problem cannot be readily solved without further elements based on physical arguments or other experiments.

In particular, it is instructive to look at the low T extrapolation of n_H and compare it to ARPES determinations of the carrier numbers, as illustrated in Fig. 5. The very good agreement found between $n_H(T = 0)$ and the number of electrons determined by ARPES strongly suggests that the low T value of $|n_H|$ corresponds to the actual value of n_e down to $x \simeq 4\%$. This implies that only electrons contribute to the transport at low T in this multi-band compound and that holes are so strongly scattered that they are not directly apparent in the transport properties.

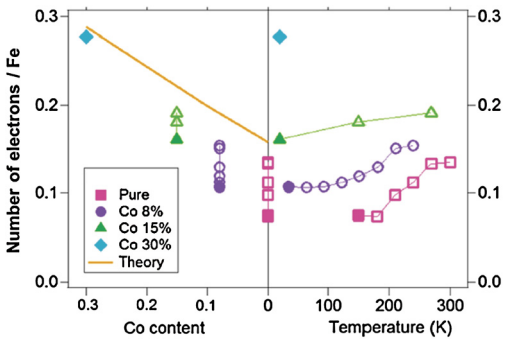

Fig. 6. Number of electrons extracted from ARPES measurements [29] as a function of the Co content for different temperatures (left) and as a function of T for different Co content (right). Thanks to the knowledge of the 3D shape of the electron pockets [22], the number of electrons can be reliably determined. The solid orange line indicates the number of electrons expected from LDA calculation.

This large asymmetry between electron and hole scattering rates has been also deduced from the analysis of electronic Raman measurements, in which different parts of the Brillouin zone can be probed by using different polarizations [34]. On the same way THz optical measurements in $Ba(Fe_{0.9}Co_{0.1})_2As_2$ clearly show that, in the normal state, the electronic contribution to the infrared and dc conductivity dominates over the hole contribution [35]. It has been shown that this disparity between electrons and holes could result from a large anisotropy of the one-particle scattering rates by spin and charge fluctuations on each Fermi surface sheet [36]. This is due both to the momentum dependence of the spin susceptibility and the multi-orbital composition of each Fermi pocket. Moreover, it is found that the longer lifetime occurs for the d_{xy} states of the electron Fermi surface sheets, where the Fermi velocity is maximum. However if forward scattering corrections due to anisotropic interband scattering off spin fluctuations are included [37], the effective transport relaxation times are found to be much more isotropic and to show no special features around the Fermi pockets.

For large Co doping, ARPES experiments show that the hole Fermi surface pockets become very small while the electron pockets significantly expand [22,23]. In this case $n_h \ll n_e$ (and $\sigma_h \ll \sigma_e$) so that Eq. (3) writes:

$$|n_H| \simeq n_e\,(1 + 2\sigma_h/\sigma) \tag{5}$$

to first order in σ_h/σ. This simple limit evidences that, whatever the exact value of n_e, the data for $\rho(T)$ and $|n_H(T)|$ would only be explained by a high T increase of σ_h with a weak minimum below 100 K. This behavior, opposite to that expected for a metallic system, led us to conclude that n_e and n_h are T dependent. This assumption has been confirmed qualitatively afterwards by ARPES measurements which reveal a strong T dependence of the electronic structure in $Ba(Fe_{1-x}Co_x)_2As_2$. A similar evolution of the electronic structure with temperature has also been observed by ARPES in $Ba(Fe_{1-x}Ru_x)_2As_2$ [33] (see below).

As shown in Fig. 6, the T dependence of the number of electrons deduced from ARPES is strikingly similar to that of $|n_H|$ reported in Fig. 4a, albeit a bit smaller quantitatively. This T variation of the carrier content can be partly assigned to the fact that E_F is only 20–40 meV below and above the hole and electron bands in the $BaFe_2As_2$ parent. Thermal population of the hole and electron bands yields then a shift of the chemical potential $\mu(T)$ to fulfill Eq. (4). A rough calculation within the Fermi liquid theory and based on a simple sketch of the Co8%–$BaFe_2As_2$ band structure gives the right order of magnitude for the observed shift of the chemical potential, supporting the idea that this effect plays a leading role [29]. Consequently, part of the T dependent band shift observed by ARPES could be a simple consequence of thermal population factors when the bottom or top of a band lies close to the Fermi energy. Nevertheless one cannot exclude that this can also be due to a weakening of the coupling between quasiparticles and interband spin fluctuations with increasing T, as the strength of the spin fluctuations is expected to decrease at high T [38].

Let us point out that an attempt to explain the sign and the temperature and doping variation of the Hall coefficient has been proposed by Fanfarillo et al. [42]. These authors show that, in a multi-band system with predominantly interband interactions between electrons and holes, current vertex corrections due to the exchange of spin fluctuations induce a mixing of the electron and hole current, which could result in a renormalized current dominated by the character of majority carrier. However this theoretical approach does not consider the possibility of a T variation of the number of carriers.

Scattering rates of the carriers and temperature dependence of the resistivity This temperature dependence of the number of carriers has important consequences on the determination of their scattering rates from resistivity measurements. Indeed in a simple metal with only one single band, the T dependence of the resistivity can be directly assimilated to the T dependence of the scattering rate of the carriers from Eq. (1). In particular it has been claimed that the linear T dependence of the resistivity observed up to ~ 120 K in $Ba(Fe_{0.93}Co_{0.07})_2As_2$ (see Fig. 1a) supports the existence of a quantum critical point on the verge of the antiferromagnetic order [39,40]. As shown above, the fact that the number of carriers increases with temperature indicates that this cannot be concluded directly from resistivity measurements. In the same way, quantum critical points have been claimed in the case of $Ba(Fe_{1-x}Ni_x)_2As_2$ for $x = 0.05$ and $x = 0.07$ on the observation of nearly linear resistivity dependences [44]. As found for Co-doped $BaFe_2As_2$ [43], the concomitant observation of an upturn in the

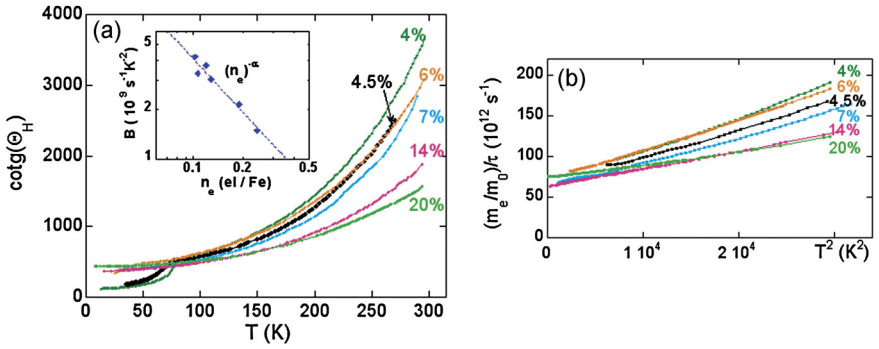

Fig. 7. (a) T variation of $\mathrm{Cot}(\Theta_H) = \rho/|R_H|$ at 1 T. (b) This quantity, which reduces to $(m_e/m_0/)/\tau$ if $\sigma_h \ll \sigma_e$, is plotted versus T^2 in the paramagnetic phase for $x \gtrsim 4\%$. This evidences a Fermi liquid behavior for $T \leq 150$ K. Inset of (a): Coefficient B of the T^2 variation versus n_e in logarithmic scales. The line corresponds to $B \propto 1/n_e$.

spin lattice NMR relaxation rate were taken as the signature of quantum criticality. Such linear resistivity dependences can also be observed in Fig. 2a for $x = 0.06$. However the analysis in a single band approach performed by these authors [44] is highly questionable; in particular, we have clearly shown that both holes and electrons contribute to the transport beyond the optimal doping [20].

In the assumption that only one electron band contributes to the transport of $Ba(Fe_{1-x}Co_x)_2As_2$, the quantity $\mathrm{Cot}(\Theta_H) = \rho/|R_H|$ equals $m_e/e\tau$ and gives a direct determination of the electron scattering rate $1/\tau(T)$. The data for $\mathrm{Cot}(\Theta_H)$ are reported in Fig. 7a for all the superconducting samples. The very similar behavior displayed by $\mathrm{Cot}(\Theta_H)$ above T_{AF} for all x does not show up any *direct* incidence on the transport of the spin fluctuations detected in the nuclear spin lattice relaxation rates [21]. This might lead us to anticipate that the variation of n_H is always governed by a T variation of n_e, even for the lower Co contents. As shown below, the interplay between charge transport and spin fluctuations can be evidenced by longitudinal magnetoresistivity measurements.

As shown in Fig. 7b for $x \gtrsim 4\%$, this yields $1/\tau(T)$ data which split, as usual, in a T-dependent $1/\tau_e(T)$ and a residual $1/\tau_0$. The former is very well fitted below 150 K by a Fermi liquid like T^2 law highly dependent on x, which excludes an electron–phonon scattering contribution. Such electron–electron scattering processes are given by:

$$\hbar/\tau_e(T) = A(k_B T)^2/E_F \tag{6}$$

where A is a dimensionless constant [41]. They are overwhelmed by phonon processes in usual metals, but are enhanced here since $k_B T \simeq E_F$. For $x = 14\%$, with $E_F = 25$ meV and $m_e/m_0 = 2$ taken from ARPES, we estimate a typical value $A \simeq 4$, which corroborates the validity of our analysis. We furthermore find that the T^2 coefficient displays a simple $1/n_e$ variation (inset of Fig. 7a), which agrees with $E_F \propto n_e^{\alpha}$ for a simple parabolic band, with $\alpha = 1$ in the 2D case. As for the disorder induced residual scattering rate τ_0^{-1}, we can see in Fig. 7b, that it remains unchanged in the paramagnetic state for all x, so that native disorder dominates over the effect of Co substitution in the Fe planes.

It is worth mentioning here that such a T^2 dependence for the scattering rate of the majority carriers has been also deduced from optical conductivity measurements [45]. Indeed the frequency-dependent conductivity can be decomposed into a broad temperature independent background and a narrow Drude-like component which solely determines the transport properties and displays a T^2 behaviour within an extended temperature range. The plasma frequency deduced from this analysis is found to be independent of temperature, which indicates that the number of carriers remains constant, in contrast to what found from Hall effect and ARPES measurements.

Spin fluctuations in the transport properties Surprisingly, as pointed out above, there is no identified signatures of the spin fluctuations in the resistivity and Hall effect of Co-doped 122 compounds in the paramagnetic state for $T > T_{AF}$. Conversely as shall be illustrated below, we have shown that the coupling between the charge carriers and the spin degrees of freedom can be revealed by high resolution measurements of the longitudinal magnetoresistivity (LMR) [46]. While a large positive LMR component is found in the AF phase of $BaFe_2As_2$, a negative and much smaller component is measured in the paramagnetic state of Co-substituted $BaFe_2As_2$ as reported in Fig. 8. The natural explanation for this negative LMR is that it results from the suppression of spin fluctuations by the magnetic field, which results in the decrease of the magnetic contribution to the resistivity. The small value of the LMR measured here (less than 0.2% at 45 K and 14 T) comforts the observation that this magnetic term plays a minor role in the value of the total resistivity.

Moreover, we observed that the dependence of the LMR coefficient $\gamma(T)$, defined as $\Delta\rho(T, H) = -\gamma(T)H^2$, with T and Co content reported in Fig. 9a mimics the behavior of the NMR relaxation rates displayed in Fig. 9b. This strongly supports the relation between the negative LMR and the AF spin fluctuations.

The T dependence of the LMR coefficient can be explained in an itinerant nearly antiferromagnetic Fermi liquid model with

$$\Delta\rho(T, H) \sim -a(T)\rho_{sf}(T)H^2 \sim -a(T)TH^2 \tag{7}$$

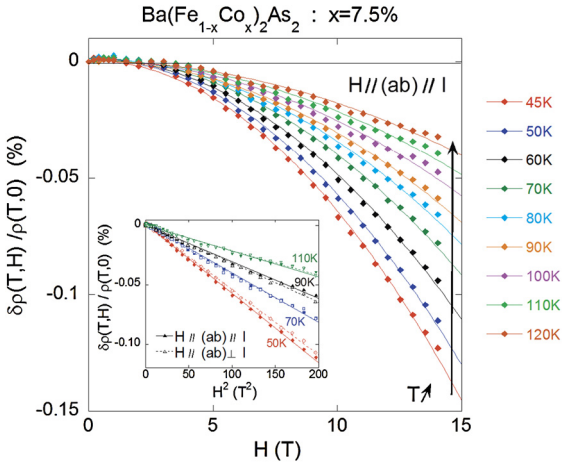

Fig. 8. Magnetic field dependence of the resistivity of the non-AF $Ba(Fe_{0.925}Co_{0.075})_2As_2$ for T ranging from 30 to 120 K for $\mathbf{H} \parallel ab$-plane and $\parallel I$. Lines are fits with a quadratic field dependence. From [46]. Inset: The longitudinal $\delta\rho/\rho_0$ values plotted versus H^2 for $\mathbf{H} \parallel \mathbf{I}$ (full symbols) or $\mathbf{H} \perp \mathbf{I}$ (empty symbols) show that the LMR is isotropic in this 7.5%Co-doped sample.

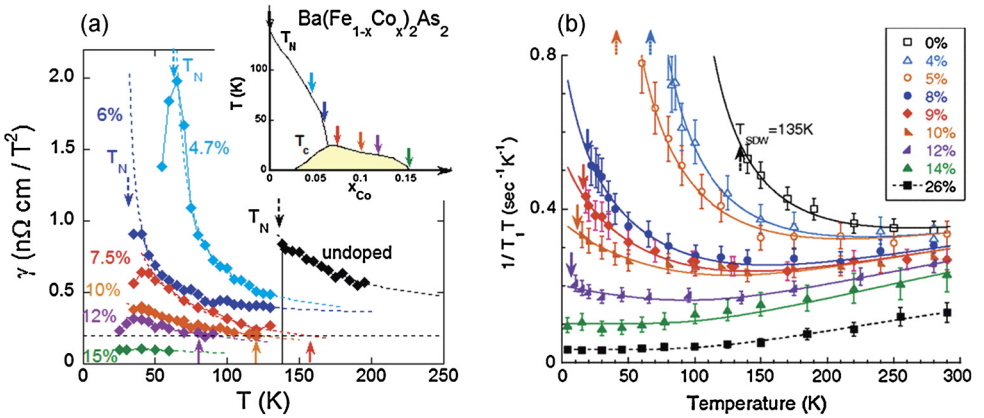

Fig. 9. (a) Temperature dependence of the longitudinal MR coefficients $\gamma(T) = -\Delta\rho/H^2$ for the $Ba(Fe_{1-x}Co_x)_2As_2$ samples whose respective positions in the phase diagram are indicated by arrows in the inset. The shape of the curves resemble those found for the ^{75}As NMR $1/T_1T$ relaxation rates displayed in (b). (b) ^{75}As NMR $1/T_1T$ relaxation rates for a similar series of $Ba(Fe_{1-x}Co_x)_2As_2$ samples. From [43]. The upgoing arrows in (a) indicate the onsets of the upturns in $1/T_1T$ observed in (b) for the same Co contents.

where ρ_{sf} is the magnetic part of the resistivity and is found to be proportional to T when the spin fluctuation spectrum is two-dimensional [47] and $a(T)$ measures the coupling effectiveness between the uniform mode at $q = 0$ and the modes with $q \approx Q_{AF}$ [48]. Good fits of our data can be obtained with

$$a(T) = \frac{1}{T - \theta} \text{ for } x < 0.075 \tag{8}$$

with $\theta \sim T_N$ for $x = 0.047$ and 0.06 and

$$a(T) = \frac{1}{(T - \theta)^2} \text{ for } x \geq 0.075 \tag{9}$$

where θ decreases slightly from 0 in the optimally doped sample to ~ -50 K in the most doped 15.4%Co one. These negative values of θ that reveal the existence of short-range AF spin fluctuations are in relatively good agreement with those extracted from INS or NMR experiments, albeit a little smaller [49,43].

These results uncover a subtle modification of the interaction between the conduction electrons and the fluctuating magnetic moments in the paramagnetic state, which occurs simultaneously with the loss of long range antiferromagnetic order at lower temperatures when T_c is optimal. This would be related to the multi-orbital nature of the iron pnictides. In underdoped compounds, strong orbital differentiation between the 3d Fe orbitals [28,50,51] results in a description in terms of coexisting itinerant and localized electrons. The situation appears then reminiscent of that encountered in s–d AF metals where the electrons in the conduction s band are the charge carriers while those in the narrow d band contribute to the spin fluctuations [47]. Beyond optimal doping, the weakening of the orbital differentiation with electron doping

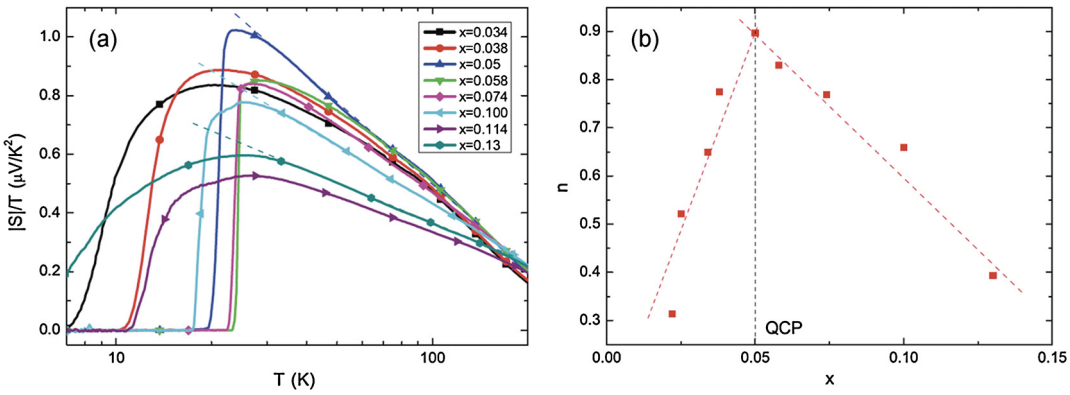

Fig. 10. (a) Temperature dependence of the Seebeck coefficient S divided by T in a series of superconducting $Ba(Fe_{1-x}Co_x)_2As_2$ samples. The dotted lines emphasize linearity on a log T scale. (b) Plot of the slope n of the logarithmic temperature dependence of S/T as a function of Co substitution x which shows an increase close to $x \simeq 0.05$. From [54].

predicted theoretically [51,52], might result in a strong hybridization between local moment and itinerant electrons and in a modification of the coupling between charge carriers and magnetic fluctuations. A more precise consideration of the characteristics and nesting properties of the different Fermi sheets is necessary to explain the quantitative evolution of the LMR in these multi-orbital compounds.

Thermopower and quantum critical point It has also been proposed that thermoelectric power (TEP) measurements can be used to probe spin fluctuations in proximity to a quantum critical point in Fe-based superconductors. When the low-energy spin fluctuations are quasi-two-dimensional, with a typical two-dimensional ordering wave vector and three-dimensional Fermi surface, the electrons are strongly scattered in the "hot" regions on the Fermi surface. This results in a logarithmic temperature dependence for the Seebeck coefficient S [53], as observed in different heavy-fermion compounds. TEP data in $Ba(Fe_{1-x}Co_x)_2As_2$ have been analysed under these lines [54]. As reported in Fig. 10, a logarithmic dependence of S/T can be observed in a small temperature range. Moreover the increase of $|S|/T$ and the slope of its logarithmic temperature dependence near $x \simeq 0.05$ was interpreted as due to an increase of scattering on nearly critical spin fluctuations.

However, the maximum of n peaks near $x = 0.05$ where a magnetic transition is still observed around 60 K (see Fig. 1). Surprisingly this transition is not visible on the TEP data and one can wonder about the meaning of a temperature logarithmic dependence between 30 and 100 K in this 5% Co-doped sample where scattering processes are expected to be very different in the magnetic and paramagnetic phases.

2.1.2. Transport in the low temperature antiferromagnetic phase

Parent compounds The drop of the resistivity in the parent compounds of the 122 systems, as seen in Fig. 1a for $BaFe_2As_2$, signals the reconstruction of the Fermi surface below the magneto-structural transition with the appearance of tiny Fermi surfaces. This has been very well evidenced by ARPES [55–59] and quantum oscillations [60–62] measurements. Transport properties in the low-T magnetic phase were analysed within a multi-band approach with different types of carriers and different mobilities [63–65]. Contrary to what is observed in the paramagnetic state, the residual resistivity ρ_s in the magnetic state is very sensitive to thermal annealings [66,65], ρ_s of as-grown samples being decreased by up to one order of magnitude by appropriate treatment as seen in Fig. 11a [65]. More importantly, the temperature dependence of the Hall coefficient in Fig. 11b is strongly affected by thermal annealing, which evidences the contribution of different electronic bands in the transport properties.

Concomitant data of resistivity, Hall effect and magnetoresistance were analysed within a multi-carriers model [63,65]. In Ref. [65], three different carriers – two electron bands and one hole band – are necessary to account for the results, in agreement with quantum oscillations results obtained on annealed $BaFe_2As_2$ [62]. One type of the electron carriers has a lower density and a higher mobility than the two other ones which display similar features. One can notice that the evolution of the Hall coefficient with annealing suggests that the hole mobility should be more sensitive to impurities, washing out the contribution of holes to the Hall effect at low T in as-grown samples. A different analysis of the magneto-transport in the magnetic phase of $BaFe_2As_2$ was proposed in [63,64] based on the observation of linear field dependence of the magnetoresistance above 1 T in as-grown samples. However measurements at much higher fields (up to 50 T) show quadratic magnetoresistance [67].

In all these analyses, the number of carriers in the different bands were considered to be independent of T. As unusual temperature effects on the electronic bands were observed by ARPES experiments in the paramagnetic phase of Ba-122 [29,33], one can expect that such temperature dependent band shifts have enhanced effects on the reconstructed Fermi surface due to the strongly reduced size of the Fermi pockets in the SDW state. In fact change in the Fermi surface topology with temperature has been proposed to explain electronic Raman scattering in the spin-density wave phase of $SrFe_2As_2$ [68]. The temperature dependence of the SDW gaps reveals an unusual evolution of the reconstructed electronic structure with

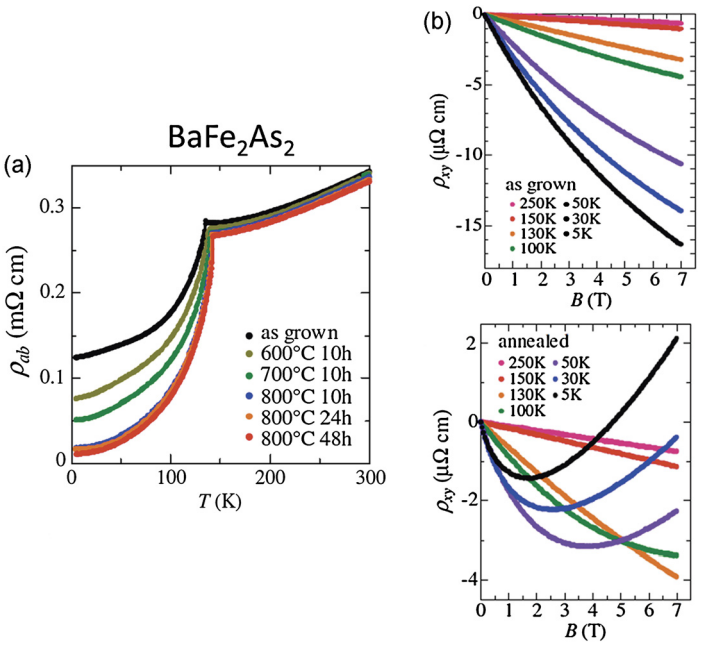

Fig. 11. (a) Effect of annealing under the various conditions shown in the figure on the in-plane resistivity curves of twinned $BaFe_2As_2$ samples. (b) Effect of annealing on the magnetic field dependence of the Hall resistivity (from [65]).

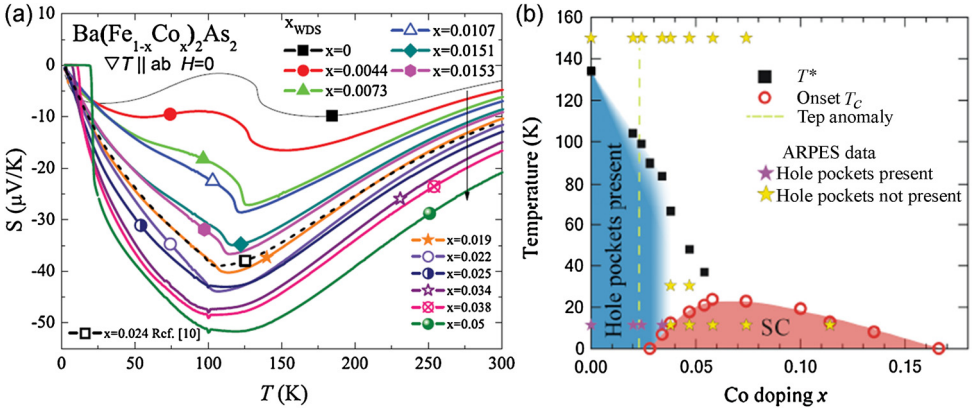

Fig. 12. (a) Thermoelectric power as a function of temperature for $Ba(Fe_{1-x}Co_x)_2As_2$ (from [69]). (b) Schematic phase diagram of $Ba(Fe_{1-x}Co_x)_2As_2$ based on transport and ARPES measurements. Green dashed line shows the doping location of the sudden change in S. The blue area represents the doping region where the reconstruction of the Fermi surface occurs (from [70]).

at least one gap being activated only well below the magnetic SDW transition T_N. This is associated with a sign change of the low field Hall coefficient R_H, from positive at high T to negative at lower T when the other SDW gap peak emerges in the Raman data. These observations have been ascribed to a temperature induced disappearance of a hole pocket, indicating a change in Fermi surface topology deep in the SDW phase [68].

Transport in the magnetic phase of electron doped 122 compounds As seen above, the topology of the Fermi surface in the SDW phase makes it particularly sensitive to external perturbations. It was found very early that a tiny electron doping of the 122 compounds has an important effect in their transport properties in the magnetic phase. In $Ba(Fe_{1-x}Co_x)_2As_2$, Hall effect and thermopower measurements [6,69] evidence a drastic change in the electronic structure for $x \simeq 0.02$, as illustrated in Fig. 12a for the Seebeck coefficient S.

As the thermoelectric power (S) is connected to the derivative of the density of electronic states, it is particularly sensitive to any modification of the Fermi surface topology. Moreover, it is found that the sudden change in S occurs near the Co doping where superconductivity emerges in the phase diagram. Subsequent ARPES measurements evidence that the Fermi surface reconstruction vanishes at this doping level, the top of the hole bands in the reconstructed Fermi surface moving below the Fermi energy, which signals the occurrence of a Lifshitz transition [56]. Superconductivity and magnetism can

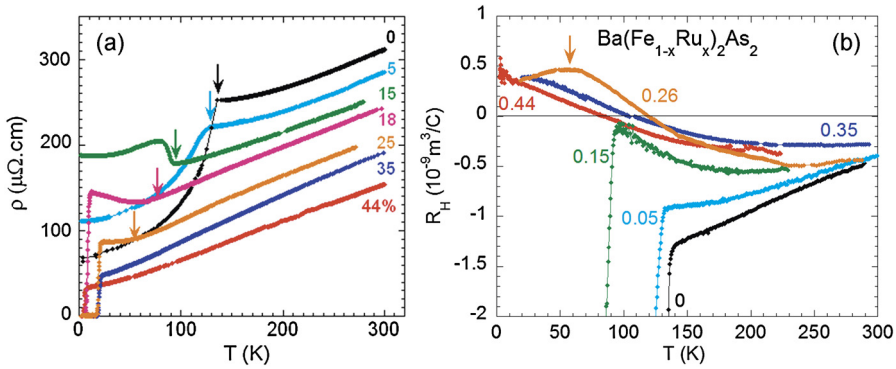

Fig. 13. (a) Temperature dependence of the in-plane resistivity $\rho(T)$ of $Ba(Fe_{1-x}Ru_x)_2As_2$ single crystals. The arrows signal the occurrence of the magnetostructural transitions. (b) Temperature dependence of the Hall coefficient $R_H(T)$ in the vicinity of $R_H = 0$ [76].

coexist only when these hole pockets are suppressed. This shows that the topology of the Fermi surface has important consequences on the superconducting and magnetic properties of these compounds (see Fig. 12b).

2.2. Isovalent substitution

Another possibility to induce superconductivity in the iron-pnictides is upon substitution by isovalent atoms, either on the Fe site by Ru atoms or on the As site by P atoms. This type of substitution does not change the balance between the electron and hole bands. The modifications of the electronic structure must be driven here by structural modifications such as the height of As with respect to the Fe planes or the value of the As–Fe–As bonding tetrahedral angle.

2.2.1. Isovalent substitution on the iron site: Ru

Ru substitution at the Fe site expands the lattice in the (a, b)-plane but shrinks it along the c direction [76,77], resulting in weaker lattice anisotropy and strong modification of the electronic structure. This is different from the effect of external pressure or P substitution at the As site which both induce a decrease in all the lattice parameters. Significant modifications of the electronic structure were indeed observed by ARPES studies [74,75]. The evolution of the temperature resistivity curves as a function of Ru content is reported in Fig. 13 for $Ba(Fe_{1-x}Ru_x)_2As_2$ single crystals [76]. Similar results were reported in [77,80]. The evolution of the $\rho(T)$ curves look like those observed for the doped samples as reported in Figs. 1a and 2a. As in electron doped $BaFe_2As_2$, the sharp drop signalling the magnetostructural transition in the parent compound evolves towards a step-like increase in resistivity when Ru is introduced. This is in contrast to what is observed in polycrystalline samples where the resistivity always decreases at the transition [11,12]. Except for the sample with a Ru content of 0.15, it is not possible to distinguish the structural and magnetic transitions T_S and T_N from resistivity measurements (see also Ref. [77]). Superconductivity appears for $x = 0.15$ and a maximum T_c of ~ 19.5 K is found for $x = 0.35$. As in the electron doped compounds, coexistence between magnetism and superconductivity is clearly evidenced with the optimal T_c occurring when long-range magnetic order is fully suppressed. However NMR studies clearly show that superconductivity coexists with AF order only in the regions where moments are smaller than $\sim 0.3\ \mu_B$, in contrast to the observation done in Co-doped samples [78,79].

The evolution of the Hall coefficient with Ru substitution reported in Fig. 13b differs from the observation done in the other compounds. Indeed, a change of sign of R_H is seen at low temperature for intermediate doping, between 0.24 to 0.55 as reported in [80]. It is also found that the thermopower exhibits a very complicated behavior as a function of temperature and Ru substitution and becomes also positive at low T for intermediate doping [81]. In a multi-band framework, this indicates that holes and electrons contribute similarly to the transport in a large temperature range. ARPES data on crystals with 35% Ru showed that the number of holes and electrons are similar, i.e., $n = n_e = n_h \simeq 0.11$ carriers/Fe [74]. It is worth pointing out that this value is significantly larger than that determined by ARPES in the paramagnetic phase of $BaFe_2As_2$: $n = 0.06(2)$ carriers/Fe [22], confirming that important modifications of the electronic structure occur upon Ru substitution. Moreover, Fermi velocities increase significantly with respect to $BaFe_2As_2$, suggesting a reduction of correlation effects.

Let us point out that Eom et al. claimed that the change of sign in R_H observed in $Ba(Fe_{1-x}Ru_x)_2As_2$ cannot be explained in a multi-band approach but rather comes from a non-Fermi-liquid-like behavior in the vicinity of the AFM phase. However some of their arguments result from miscalculations. In particular, using a carrier density of 0.15 electrons/Fe, they found $1/ne = 0.98 \cdot 10^{-3}$ cm^3/C while a right calculation would give $2.12 \cdot 10^{-3}$ cm^3/C.[1] Consequently, contrary to what is asserted in this paper [80], the mobilities of holes and electrons are comparable at high T while that of the holes slightly overcomes that of the electrons at low T. Moreover these authors speculated that their magnetoresistance data, always lower than 1%

[1] Knowing that the cell volume of $BaFe_2As_2$ ($V = 0.204$ nm^3) contains two Fe_2As_2, a number of carriers of $n = 0.15$ carriers/Fe corresponds to $2.94 \cdot 10^{27}$ carriers/m^3, resulting in a Hall coefficient equal to $R_e = 1/ne = 2.12 \cdot 10^{-9}$ m^3/C or $2.12 \cdot 10^{-3}$ cm^3/C.

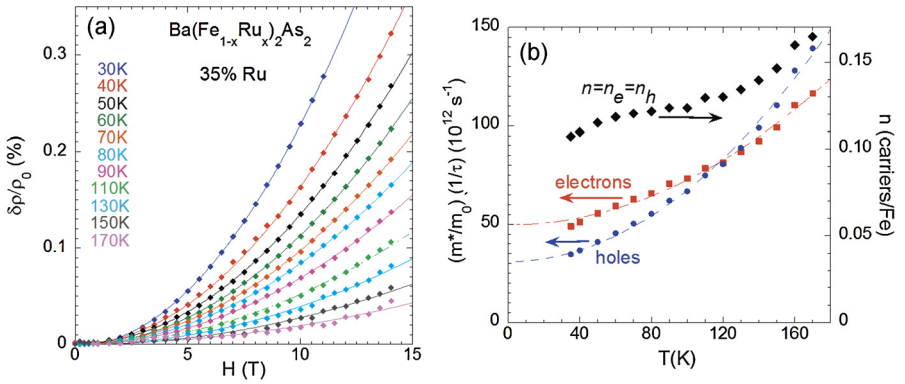

Fig. 14. (a) Transverse magnetoresistance ρ/ρ_0 for a $Ba(Fe_{1-x}Ru_x)_2As_2$ single crystals with 35%Ru at different temperatures. Solid lines are quadratic fits of the data. (b) Temperature dependence of the number of carriers and of the hole and electron scattering rates determined from resistivity, Hall coefficient and magnetoresistance data as explained in the text. Dotted lines are quadratic fits of the data showing that both the electrons and holes exhibit a Fermi liquid behavior [82].

at 14 T, are much smaller than those predicted by a two-band model for which "a large MR is expected as long as the electron and hole carriers coexist and their mobilities are comparable". However, we do not understand how these latter values were estimated by Eom et al. [80]. Solving the problem in the opposite way, it is possible to determine directly the hole and electron conductivities σ_h and σ_e and the number of carriers $n = n_h = n_e$ from measurements of resistivity, Hall effect and magnetoresistance using the following equations:

$$\begin{aligned} \sigma &= \frac{1}{\rho} = \sigma_h + \sigma_e \\ R_H &= R_e \frac{\sigma_h - \sigma_e}{\sigma_h + \sigma_e} \text{ with } R_e = 1/n|e| \\ \frac{\Delta\rho_0}{\rho} &= R_e^2 \sigma_e \sigma_h H^2 \end{aligned} \tag{10}$$

Combining these equations one finds that the magnetoresistance writes as:

$$\frac{\Delta\rho}{\rho_0} = \frac{1}{4}(R_e^2 - R_H^2)\left(\frac{H}{\rho_0}\right)^2 \tag{11}$$

This equation is important as the proportionality between the magnetoresistance and $(H/\rho_0)^2$ has often be taken as an indication that the so-called Kohler law is obeyed or not. In multi-band systems with $n_e = n_h$, Eq. (11) tells us that this proportionality can be observed if $R_e^2 - R_H^2$ is weakly T dependent, that is for $R_e \gg R_H$ or R_H nearly constant with T. Consequently the observation or not of the "Kohler law" must be considered with caution and no rapid conclusion can be drawn.

We displayed in Fig. 14a our own data of the orbital magnetoresistance for a single crystal of $Ba(Fe_{1-x}Ru_x)_2As_2$ with 35%Ru [82]. These data are very similar to those reported by Eom et al. [80] for an optimally doped crystal. Using resistivity, Hall coefficient and magnetoresistance data, Eqs. (10) make it possible to determine the temperature dependences of the number of carriers and the scattering rates for holes and electrons that are reported in Fig. 14b. The number of carriers $\sim 0.12(1)$ electrons/Fe between 50 and 150 K is in very good agreement with that found by ARPES measurements ($n =$ 0.11 carriers/Fe) at 20 K on similar crystals [74]. This gives some confidence to this analysis in terms of two electronic bands. Let us also notice that the small increase in n for $T > 120$ K is compatible to modifications of the electronic structure with T as observed by ARPES measurements [33]. Moreover the scattering rates of both electrons and holes exhibit a T^2 dependence as also found for $Ba(Fe_{1-x}Co_x)_2As_2$, demonstrating once again that direct conclusion from the T dependence of resistivity must be considered with caution in these multi-band systems.

It is worth noticing here that the scattering rates ($\sim 5 \cdot 10^{13}$ s^{-1}) of both electrons and holes are of the same order as that of electrons in $Ba(Fe_{1-x}Co_x)_2As_2$ (see Fig. 7). Moreover the hole mobility overcomes that of electrons at low T, which implies that some scattering processes responsible for the low mobility of holes in $BaFe_2As_2$ are considerably reduced by the introduction of Ru. This is quite surprising a priori as Ru substitution would have been expected to result in strong disorder scattering. However ARPES measurements reveal a homogeneous electronic structure and no strong disorder associated with Ru substitutions. Moreover, it appears that Ru substitution also strongly weakens the electron correlations both in electron and hole bands, which can explain the increased mobility of holes in BaFeRuAs compared to BaFeCoAs [74]. By taking into account disorder effects in first-principles calculation, it was shown that, while large scattering is found on the entire Fe bands, the states near the chemical potential remain very sharp and coherent [83]. This exotic behavior originates from a coherent interference of on-site and off-site disorder potentials. This insensitivity to impurity scattering provides

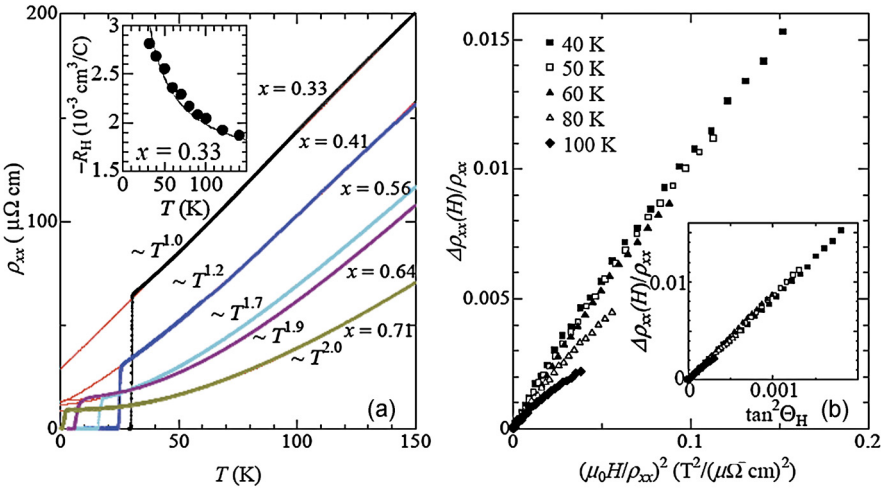

Fig. 15. (a) Temperature dependence of in-plane resistivity $\rho(T)$ of $BaFe_2(As_{1-x}P_x)_2$ for x ranging from 0.33 to 0.71. The red lines are the fit of normal-state resistivity to power-law dependence $\rho_0 = AT^\alpha$. Inset: Temperature dependence of $-R_H(T)$ for $x = 0.33$. (b) Magnetoresistance $\Delta\rho_{xx}/\rho_{xx}$ plotted as a function of $(\mu_0 H/\rho_{xx})^2$ for $x = 0.33$. The inset shows $\Delta\rho_{xx}/\rho_{xx}$ versus $\tan^2\theta_H$. From [16].

a natural explanation of the unusual resilience of transport and superconductivity against a high impurity level in this $Ba(Fe_{1-x}Ru_x)_2As_2$ system.

2.2.2. Substitution on the As site: P

The structural modifications induced by P substitution at the As site are very similar to those of hydrostatic pressure. P substitution reduces all the axis lengths and the pnictogen height z_{Pn} relative to the FeAs layers [14–16]. According to density functional theory (DFT), the hole pockets are quite sensitive to this pnictogen position. Indeed a strong increase in the warping of one hole sheet was evidenced by ARPES measurements, which would lead to weaken the nesting between the electron and hole Fermi surfaces [86]. Among the 122 compounds, $BaFe_2(As_{1-x}P_x)_2$ was particularly studied as it was considered as the ideal system to study the quantum criticality in iron pnictides (for a review, see [85]). Since substitution takes place outside the FeAs layers, the scattering rate of the defects introduced by P substitution was shown to be particularly low, as demonstrated by the observation of quantum oscillations in a wide range of P concentrations [84]. This gave rise to a lot of different studies of transport, magnetic, specific heat, ... properties.

The first assertion of quantum criticality was claimed from resistivity measurements [14–16]. As shown in Fig. 15a, the in-plane resistivity ρ displays a linear temperature dependence for $x = 0.30$ corresponding to the maximum value of T_c [16]. The authors also note that the Hall coefficient is remarkably enhanced at low temperature (see figure in Fig. 15b) and that the magnetoresistance reported in Fig. 15c violates Kohler law. All these results were taken as indicative of non-Fermi liquid behavior and the proximity of a quantum critical point.

Besides, recent measurements using high magnetic field to suppress superconductivity have revealed a T^2 behavior at low temperature for all compositions ($x \geq 0.32$) and a crossover towards a linear temperature dependence as T is increased, consistent with a Fermi-liquid ground state at low T [87]. As optimal doping is approached from the overdoped side, the range of T over which T^2 behavior is observed decreases. Good fits of the resistivity curves are done with a power law expression $\rho(T) = \rho_0 + AT^n$, with the coefficient A being strongly peaked at T_c^{max}, which was interpreted by the authors as the proximity to a quantum critical point.

However all these conclusions were drawn while considering a single band picture to describe the transport properties of $BaFe_2(As_{1-x}P_x)_2$. It is worth noting here that the same miscalculation in the estimate of $R_e = 1/ne$ as done in Ref. [80] for BaFeRuAs led the authors to conclude that the simple multi-band picture cannot be applied. The actual value of R_e, equal to $2.05 \cdot 10^{-9}$ m^3/C is in fact very close to the measured value of R_H (see footnote p. 11). Moreover, as pointed out above in the case of BaFeRuAs, the apparent violation of Kohler's law for a two-band system can very simply derive from Eq. (11) if $(R_e^2 - R_H^2)$ is dependent on T. Consequently, ruling out multi-band effects to explain the transport properties of $BaFe_2(As_{1-x}P_x)_2$ appears not really legitimate here.

As in $Ba(Fe_{1-x}Co_x)_2As_2$, the Hall coefficient is negative, indicating that the electron scattering rates must be smaller than that of holes. As a matter of fact, only two electron sheets can be revealed by quantum oscillation measurements in overdoped $BaFe_2(As_{1-x}P_x)_2$. Using the same approach as done above for BaFeRuAs, it is possible to determine the number of carriers and the scattering rates of electrons and holes from the data of resistivity, Hall coefficient and magnetoresistance reported in Fig. 15. The number of carriers found from such a decomposition is ~ 0.06 carriers/Fe, in a very good agreement with that determined by quantum oscillation measurements [84].

Even if the existence of a quantum critical point deduced from the analysis of the transport properties in a single band approach must be considered with caution as shown above, it is important to point out that the presence of a QCP in

the P substituted $BaFe_2As_2$ compound has been suggested by several other magnetic and thermodynamic measurements [88,89,84,90].

The effect of P substitution was also reported for the parent compound $EuFe_2As_2$ [91–94] in order to study the interplay between superconductivity and Eu^{2+} magnetism. As for $BaFe_2As_2$, the introduction of P results in the suppression of the antiferromagnetic phase and the apparition of superconductivity in a rather narrow superconducting dome, between $x \simeq 0.16$ and $\simeq 0.23$. The magnetic structure of Eu^{2+} was carefully investigated in Ref. [93] and the authors conclude that the development of superconductivity is supported by the decoupling of the magnetic Eu^{2+} layers. The electrodynamic in plane response of a series of $EuFe_2(As_{1-x}P_x)_2$ single crystals was studied using Fourier-transform infrared spectroscopy. The results are detailed in Ref. [94] in this volume.

2.3. *Hole doping – substitution at the alkaline earth site of* $AEFe_2As_2$, AE = Ba, Sr *or* Ca

The only possibility to induce superconductivity by hole doping in the 122 system is by alkali metal substitution in the insulating blocking layers. Indeed substitution at the Fe site by elements at the left of Fe, as Mn or Cr, which would formally lead to hole doping, fails to induce superconductivity [95,96]. In the case of Mn substitution, it has been demonstrated that the additional holes given by Mn do not delocalize but act as local moments on Mn sites with strong stabilization of the antiferromagnetic order [97,98]. However Hall effect measurements clearly show a change of sign in R_H from negative to positive upon Cr and Mn substitution, indicating that holes are actually added [95,99]. For the electron doped 122 family, such as $Ba(Fe_{1-x}Co_x)_2As_2$, experimental and theoretical works illustrate the systematic evolution of the transport properties and electronic structure; they all highlight the importance of multi-band effects. The detailed investigations and analyses suggest asymmetric quasiparticle scattering in the hole and electron bands, with still a much larger mobility in the electron band. Detailed studies of the Hall resistivities in Mn-substituted $BaFe_2As_2$ as well as simultaneous analyses of both longitudinal and transverse magnetoconductivities demonstrated that minor number of holes with high mobility were generated by the Mn doping, while the majority electron and hole Fermi surfaces in the electronic structure of the parent $BaFe_2As_2$ were almost preserved [100]. Where are located the minority holes is not yet clearly elucidated.

Hole doping is then achieved by substitution of K or Na at the alkaline earth site, the most studied compound being $Ba_{1-x}K_xFe_2As_2$. Compared to its counterpart electron doped $Ba(Fe_{1-x}Co_x)_2As_2$, there are relatively few systematic studies of transport properties all along the phase diagram, due to the larger difficulty to grow good single crystals with a narrow compositional distribution especially for heavily K doped crystals

The evolution of the resistivity curves reported in Fig. 16a shows up some differences from the observations done in electron doped compounds [101]. First, the drop of resistivity which signals the magneto-structural transition at 138 K in the parent compound is shifted to lower temperature upon K substitution but without strong modification of the $\rho(T)$ curves: the derivatives of the resistivity always display a unique peak, showing that the magnetic and structural transitions take place at the same temperature as evidenced by X-rays and neutron diffraction measurements [102]. The shape of the resistivity curves is also very different: in K substituted $BaFe_2As_2$, resistivity curves exhibit a crossover from a low-T positive to a high-T negative curvature contrary to the case for the other types of substitution. Moreover, one can see that the $\rho(T)$ curves remain almost unchanged once the superconductivity sets in. Resistivity measurements performed for a large range of hole doping show that the room-temperature resistivity $\rho(300\ K)$ remains constant, within statistical error, over the whole composition range from heavily underdoped samples with $x = 0.22$ to heavily overdoped $x = 1$ [103,104]. This is very different from what is observed in the other types of substitution (see Figs. 1, 2, 13 or 15), for which $\rho(300\ K)$ decreases notably with doping. By contrast, one observes that the Hall coefficient R_H exhibits a significant modification with K content, as seen is Fig. 16b. In particular, a change of sign in R_H is observed as soon as K is introduced, indicating that the contribution of holes rapidly overcomes that of electrons. Moreover one can notice that the crossover temperature, where R_H turns to a decrease upon cooling is rather close to the crossover seen in resistivity.

These results were usually discussed in a two-band approach. However, to our knowledge, there were no attempts to analyse resistivity and Hall coefficient data simultaneously as a function of x and T in order to get the rough evolution trends of the different parameters defined in Eq. (3). In particular, the saturation of the $\rho(T)$ curves at high T was interpreted by an effect of "shunting", with the conductivity of one band being strongly T dependent, while the other is nearly T independent [106,101]. One can notice that optical conductivity data have been often interpreted along these lines [105,45,107]. Two Drude terms, representing two groups of carriers with different scattering rates have been used to describe the real part of the optical conductivity with a "broad" Drude component with a T-independent scattering rate, and a "narrow" Drude T dependent component. In the case of the optimally doped $Ba_{0.6}K_{0.4}Fe_2As_2$, the scattering rate of the "narrow" Drude peak was found to increase linearly with T from 50 to 300 K, suggesting the presence of a quantum critical point into the superconducting dome [107]. However, direct fits of the $\rho(T)$ curves using a power-law dependence $\rho(T) = \rho_0 + AT^n$ as done in P-substituted $BaFe_2As_2$ [61] did not give conclusive results. Although the exponent n is found to be minimum (~ 1.1–1.5) for $x = 0.39$ with maximum T_c, negative values are obtained for the residual resistivity ρ_0, which indicates that this fitting procedure must be considered with caution [101,103,104].

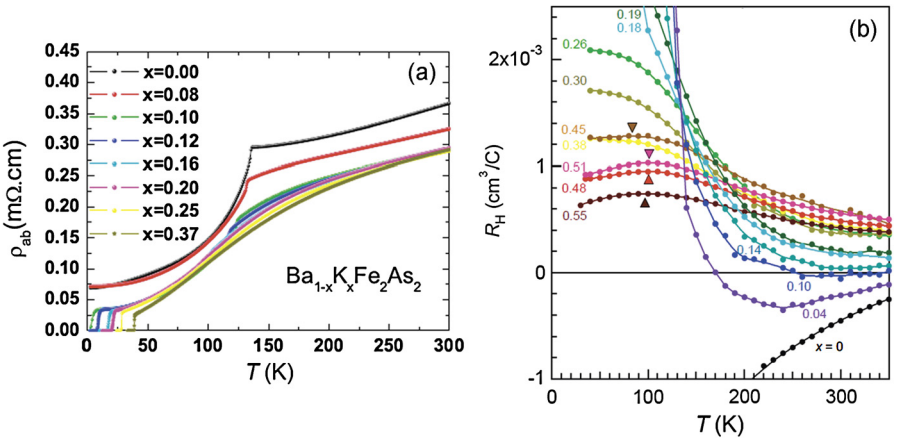

Fig. 16. (a) Temperature dependence of resistivity of $Ba_{1-x}K_xFe_2As_2$ ($x = 0$ to 0.37) single crystals. The magneto-structural transition is shifted to lower temperatures and becomes rounded with further potassium doping. The resistivity anomaly in the normal state cannot be explicitly resolved when the doping level is 0.25 with $T_c = 29$ K and beyond, from [102]. (b) Temperature dependence of the Hall coefficient R_H for $0 \leq x \leq 0.55$. The triangles indicate the crossover temperature, where R_H turns to a decrease upon cooling. From [103].

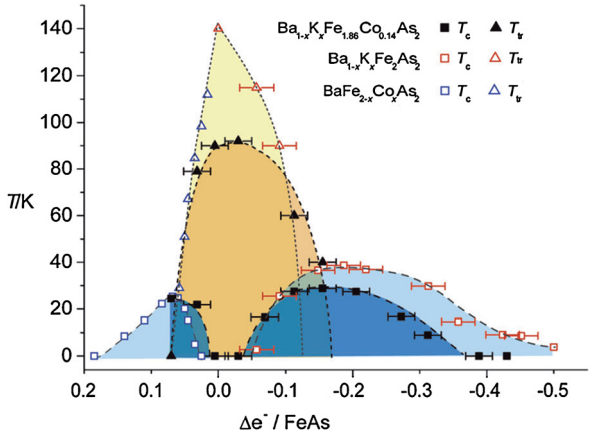

Fig. 17. Phase diagram of $Ba_{1-x}K_x(Fe_{0.93}Co_{0.07})_2As_2$ (dark blue/orange) compared to the phase diagrams of $Ba_{1-x}K_xFe_2As_2$ and $Ba(Fe_{1-x}Co_x)_2As_2$ (light blue/yellow). From [109].

2.4. Comparison between the different types of substitution

2.4.1. Role of disorder

Value of T_c It has been often suggested that T_c is higher in the hole-doped than in the electron-doped Ba-122 compounds due to more disorder effects in the latter case, where the dopants are located in the FeAs layers (see for instance [18] in this volume). It was indeed shown that the chemical nature of the substitution in the FeAs layer has an important influence on the superconductivity and the transport properties. For instance Ni (Pd) substitution in the Ba or Sr-122 systems results in lower maximum T_c than Co (Rh) substitution [20,26]. This has been interpreted as a stronger pair breaking effect for Ni or Pd substitution than for Co [108].

However it is not so straightforward to assert that lower T_c in Co-substituted samples as compared to K-substituted samples is exclusively due to disorder effects since the electronic structures are very different in these two cases. Indeed the phase diagrams are asymmetric for electron and hole dopings, which may indicate that the excess positive and negative charges act differently. A very interesting experiment of co-doping using the combination of both K and Co substitutions in $Ba_{1-x}K_x(Fe_{0.93}Co_{0.07})_2As_2$ [109] have clearly evidenced that the charge in the FeAs layers plays a major role in controlling the shape of the phase diagram of the Ba-122 compound. As reported in Fig. 17, the emergence of superconductivity and the disappearance of the magnetic phase are only dependent on the effective charge given to the FeAs layer. However, one can notice that the maximum T_c in the hole-doped part of the phase diagram is higher than in the Co samples, which has been interpreted as the effect of disorder introduced by the Co substitution in the iron layer.

Nevertheless one can point out that, in our analysis of transport data in $Ba(Fe_{1-x}Co_x)_2As_2$, the scattering rates of electrons at low T do not depend on the Co content from 4% to 20% Co (see Fig. 7b), which led us to conclude that native disorder dominates over the effect of Co substitution [6]. Moreover, Katase et al. [110] showed that the superconducting

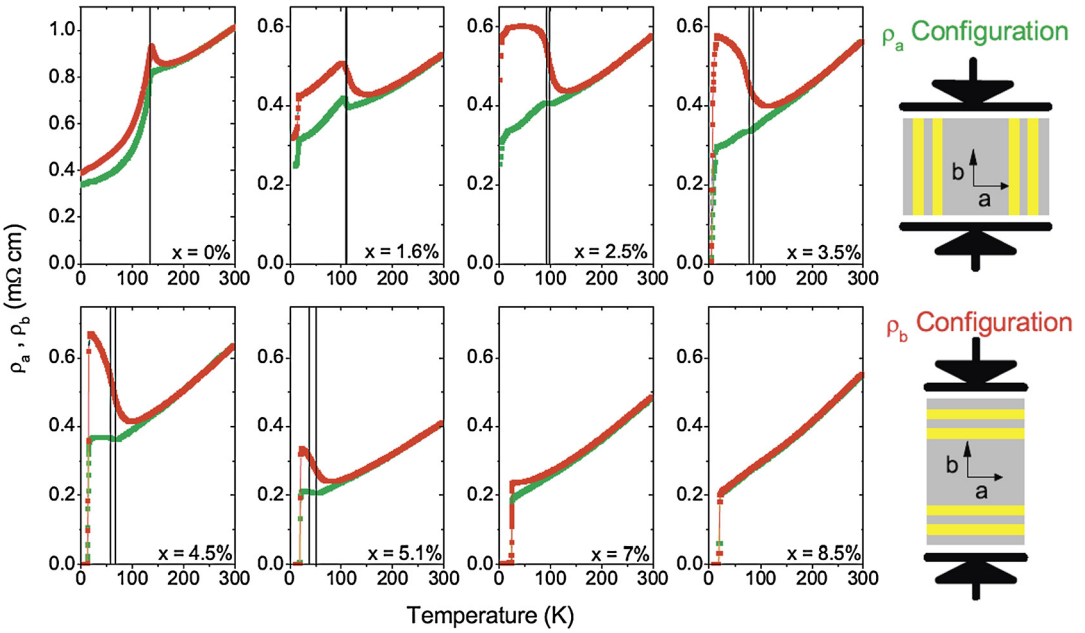

Fig. 18. Temperature dependence of the in-plane resistivity ρ_a (green) and ρ_b (red) of $Ba(Fe_{1-x}Co_xx)_2As_2$ for Co concentrations from $x = 0$ to 0.085. Solid vertical lines mark critical temperatures for the structural and magnetic phase transitions T_S and T_N, respectively. The diagrams on the right illustrate how measurements of ρ_a and ρ_b were made. Dark arrows indicate the direction in which uniaxial pressure was applied, and smaller arrows indicate the orientation of the a and b crystal axes. From [71].

dome of epitaxial films of La-doped $BaFe_2As_2$ closely overlaps with that of Co-doped $BaFe_2As_2$, leading them to conclude that T_c does not depend on whether or not impurity dopants are located in the FeAs layer but only depends on the excess charges provided by the dopants. This result also suggests that the differences observed in Fig. 17 in the hole doped area of the phase diagram between $Ba_{1-x}K_xFe_2As_2$ and $Ba_{1-x}K_x(Fe_{0.93}Co_{0.07})_2As_2$ is not due to disorder effects induced by Co substitution but must be related to differences in the magnitudes of superconducting interactions for the hole and electron doped $BaFe_2As_2$.

Impurity scattering and resistivity anisotropy above T_N in the underdoped area of the phase diagram As we have shown above, the resistivity drop which signals the occurrence of the magnetostructural transition in the parent compound $Ba(Sr)Fe_2As_2$ transforms into a step-like increase in the resistivity as soon as Co or Ni are inserted in the FeAs layers (see for instance Fig. 1 [6] and Fig. 2 [20]) or by P substitution on the As site [16]. However, no increase of resistivity was observed in the hole doped K-substituted compounds (see Fig. 16 [101,111]).

Resistivity measurements in the presence of uniaxial stress have showed that this increase in resistivity results predominantly from the resistivity component along the b-axis which is found to be larger than along the a-axis in the electron doped Ba-122 [71,64,73]. This anisotropy of resistivity in the tetragonal phase is however much reduced in the hole doped $Ba_{1-x}K_xFe_2As_2$ and also changes sign for sufficiently high dopings [111,112]. This in-plane resistivity anisotropy which is observed above the structural transition T_S has been taken as the hallmark of a nematic state in iron-pnictides (Fig. 18).

In one hand, by comparing Co and Ni doped samples, it has been argued [72] that the resistivity anisotropy does not depend on impurity concentration and is thus an intrinsic property determined by the Fermi surface anisotropy. On the other hand it was shown by Ishida et al. that the resistivity anisotropy is strongly dependent on the quality of the samples [73], which tends to suggest that it is more likely extrinsic in origin and comes from anisotropic scattering potentials induced by Fe vacancies and Co defects in the antiferromagnetic phase.

Models based on spin-fluctuation scattering in presence or not of strongly anisotropic impurity states [115,37,113,114] were proposed to explain these different types of behaviors. Within scenario which privileges the role of scattering off elongated ("nematogen") defects, the much larger anisotropy in electron-doped Ba-122 compared to hole-doped Ba-122 is explained as a consequence of the presence of dopants within the iron planes. In the latter case, the smaller and negative anisotropy might arise from peculiar features in the electronic band structure.

The origin of this resistivity anisotropy is still an ongoing debate whose discussion constitutes the entire subject of other contributions in this volume [116,117]. Thus we will not detail this issue here and recommend the interested readers to look at these papers.

Interplane resistivity All the resistivity data reported up to now have concerned the in-plane ρ_{ab} resistivity, along the FeAs layers. Indeed quite few works have been devoted to the study of the interplane ρ_c resistivity. This is likely due to the

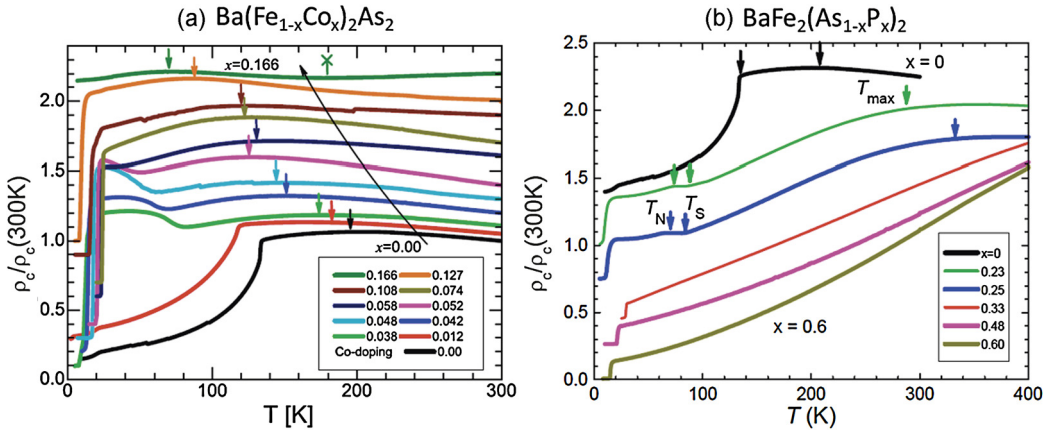

Fig. 19. Temperature dependence of the interplane resistivity ρ_c for $Ba(Fe_{1-x}Co_x)_2As_2$ (a) and $BaFe_2(As_{1-x}P_x)_2$ (b) (from [118,121]). While T_{max} (arrows) decreases with Co doping in (a), it increases and rapidly disappears in the case of P substitution.

difficulty to extract good absolute resistivity values in this case [118]. A systematic study of the temperature dependence of ρ_c in different hole and electron doped Ba-122 was performed by Tanatar et al. [118–120]. In all cases, ρ_c displays a shallow crossover maximum at T_{max}, followed by a broad minimum at higher temperature above which ρ_c increases linearly with temperature (see Fig. 19). None of these features are apparent in the in-plane resistivity. In BaFeCoAs [118], the T dependence of the interplane resistivity show some correlation with the NMR Knight shift and spin lattice relaxation rate, which was assigned to the formation of a pseudogap [43]. It was thus concluded that the T dependence of ρ_c constitutes a good probe to detect the presence of a pseudogap in iron pnictides. However, while in electron-doped compounds [118,119], this "pseudogap" region extends from parent compound to far beyond the end of the superconducting dome with a rapid suppression of T_{max} with doping [118], the maximum in ρ_c shifts to higher temperatures in hole doped Ba-122 [120] and isoelectronic P or Ru substituted samples [121,122] in which it disappears very rapidly with doping: at the optimal doping, ρ_c shows T-linear temperature dependence without any crossover anomalies.

On the other hand, infrared studies of the a–b-plane response in Co and P substituted $BaFe_2As_2$ [123] and of the c-axis response in optimally doped BaFeCoAs [124] identify a suppression of the spectral weight at low frequencies, which is reminiscent to the spectroscopic manifestations of the pseudogap in the cuprates. Opening of a pseudogap was also reported via optical conductivity in underdoped $Ba_{1-x}K_xFe_2As_2$ [125]. However all the analysis of the optical response was performed there in a single band approach. It was pointed out in Ref. [124] that the multi-band character of the iron pnictides is likely to also play a role in the suppression of the spectral weight. In particular, detailed calculations evidence a role of multi-band effects in the spectral weight redistribution in iron-pnictides [38].

In conclusion, the T dependence of the interplane resistivity $\rho_c(T)$ and the interlayer charge dynamics in iron pnictides appears to be far from being well understood and calls for further theoretical analysis. Let us mention here that the T dependence of ρ_c is very similar to that measured in Sr_2RuO_4, another multi-band compound where "metallic" conduction is also observed at high T in a regime with no coherent band formation [126]. This poses the question of the nature of the quasiparticles that contribute to the c-axis transport in these anisotropic compounds. This issue clearly deserves further investigations.

3. 111 compounds

3.1. LiFeAs

Among the iron pnictides, the LiFeAs compound occupies a special place in various aspects. First it is naturally superconducting with a relatively high $T_c \sim 18$ K without any chemical doping. Cleaved single crystals display no surface states, which makes it very appropriate for ARPES measurements. It has been shown that the nesting between hole and electron Fermi pockets is very poor, which has raised the question of the role of antiferromagnetic fluctuations for superconductivity in this compound [127,128].

Due to reduced defect content, the residual resistivity in LiFeAs is found to be quite low with residual resistivity ratio much larger than found in the other pnictide compounds [129–131]. The low temperature resistivity follows a quadratic T dependence, which is a clear indication of Fermi liquid behavior with electron–electron scattering. The Hall coefficient R_H is negative indicating that the transport properties are dominated by electrons in this nearly compensated material, as found in the non-magnetic state of $BaFe_2As_2$ [6]. As a function of temperature, R_H exhibits a significant temperature dependence with a minimum around 100 K and a saturation towards zero with increasing T, which signals that the mobilities of holes and electrons become similar.

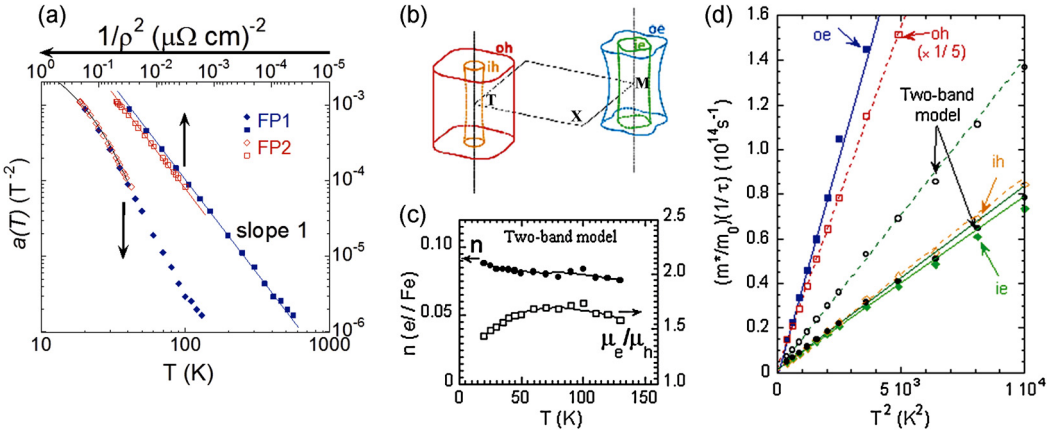

Fig. 20. (a) The MR coefficient $a(T)$ of Eq. (12) is plotted versus T and $1/\rho^2$ for two different single crystals. The full lines of slope 1 indicate that Kohler's rule is very well obeyed (see text). (b) Schematic view of the Fermi surfaces sheets of LiFeAs. (c) Number of carriers and mobility ratio extracted from the compensated two-band model. (d) Scattering rates deduced in a two-band analysis (circles) and for the four-band solution given in the text, plotted versus T^2. Full (empty) symbols and full (dashed) linear fits are for the electrons (holes). Notice that the data for the oh band has been divided by 5.

Taking benefit of the reduced defect content, we were able to follow the evolution of the transverse magnetoresistance (MR) up to 160 K [131]. For $T \gtrsim 45$ K, the MR increases as H^2 in the whole field range investigated ($H \leq 14$ T). Some deviations occur at lower T and low field, which can be assigned to the contribution of superconducting fluctuations, the quadratic behavior being fully restored beyond a threshold field $H'_c(T)$, allowing us to define the MR coefficient $a(T)$ as

$$\delta\rho/\rho(T,0) = [\rho(T,H) - \rho(T,0)]/\rho(T,0) = a(T)H^2 \tag{12}$$

As shown in Fig. 20a, $a(T)$ is found to decrease by about three orders of magnitude from T_c to 160 K.

The Fermi surface of LiFeAs determined by ARPES measurements [127,128] shows that hole carriers are located in a small inner (ih) band included in a large outer (oh) band. Similarly, it has been shown that, due to strong spin-orbit coupling, the electron bands split into an inner (ie) band included in an outer one (oe) [132,133]. A schematic view of the Fermi surfaces sheets is reported in Fig. 20b. There is a good agreement with electronic structure calculations if electronic correlations are taken into account [51,3]. Moreover, as expected for an undoped pnictide, one finds equal number of electrons and holes $n_e = n_h = n \simeq 0.2$ carriers/Fe [127,128].

3.1.1. Compensated two-band model

The easiest approach is first to assume that the respective mobilities of holes and electrons are similar in the different hole and electron bands, allowing us to analyse the transport data within a two-band with $n_e = n_h$. The transport coefficients are then given by Eqs. (10) and (11), which permits us to deduce the T variations of the number of carriers n and their respective mobilities μ_h and μ_e.

We can see in Fig. 20a that $a(T)$ scales as ρ^{-2}, that is Kohler's rule is well obeyed in LiFeAs. According Eq. (11), this indicates that $R^2 - R_H^2$ (with $R = 1/n|e|$) has a weak T dependence. We show in Fig. 20c that both scattering rates display a T^2 variation up to ~ 70 K, with $\mu_e/\mu_h \sim 1.5$ (see Fig. 20c),[2] and that the number of carriers is nearly T independent below 120 K.

3.1.2. Comparison with ARPES and dHvA: beyond the two-band model

However, the deduced carrier content $n \sim 0.09$ *el*/Fe being twice smaller than that given by ARPES or by dHvA [128,134], this implies that the two-band model only allows us to determine separate average parameters for the holes and electrons. If the carrier mobilities differ substantially for the different four bands, it is necessary to write the MR coefficient using a more complicated expression than given in Eq. (11) [64], which takes into account the number of carriers in the different bands and their respective mobilities. This analysis is detailed in Ref. [131]. For hole or electron bands, the key parameters are the effective mobility (μ_h and μ_e) and the effective number of carriers (n_h and n_e), which depend both on the mobilities and on the number of carriers in the different bands. To approach a solution we have used for the T-independent carrier contents those obtained from ARPES and dHvA experiments $n_{oh} \sim 0.16$ *h*/Fe, $n_{ih} \sim 0.03$ *h*/Fe, $n_{oe} \sim 0.11$ *el*/Fe and $n_{ie} \sim 0.08$ *el*/Fe for the outer and inner hole (electron) bands respectively. As we are still lacking sufficient experimental information, a unique solution cannot be acquired. However dHvA results imply that the mobilities for the two electron bands are comparable.

[2] The values of the electron and hole mobilities, and their ratio, determined here are very different from those reported in Ref. [130] in which $\mu_e/\mu_h \sim 10$. We do not understand this difference as their raw data are very similar to ours. A correct estimate would give $\mu_e/\mu_h \sim 1.4$.

Matching the data with all these assumptions yields a strong differentiation of the two hole bands with a surprisingly much lower mobility for the outer band compared to the inner one. Also, imposing $\mu_{oe} \simeq \mu_{ie}$ puts some constraints on the value of n_h^{eff} that cannot be larger than ~ 0.06 h/Fe. A solution with $n_h^{eff} = 0.05$ h/Fe whatever T is illustrated in Fig. 20d and gives a ratio between the electron (hole) mobilities respectively of $\mu_{ie}/\mu_{oe} = 3$–6 and $\mu_{ih}/\mu_{oh} \sim 17$. It corresponds to $n_e^{eff} \sim 0.13$ el/Fe and it results in similar values of the effective electron and hole mobilities, which would justify why Kohler's rule is obeyed in this compound. Whatever the value taken for n_h^{eff} in the range considered, we always find that the scattering rates for the different carriers increase as T^2 up to ~ 70 K, as seen in Fig. 20d. This confirms a Fermi liquid behavior for both holes and electrons in agreement with density functional theory and dynamical mean Field (DFT + DMFT) calculations [132].

For the outer hole band, ARPES measurements [135] allow us to determine directly the electronic scattering rate $(m^*/m_0)(1/\tau) \sim 8 \cdot 10^{13}$ s^{-1} which is in a fairly good agreement with $\sim 2 \cdot 10^{13}$ s^{-1} found here by transport. Measurements of the lifetimes for the other pockets should be very interesting.

3.1.3. Manifestation of spin fluctuations

As reported above, measurements of the longitudinal magnetoresistance provide a useful probe for studying the coupling between the charge carriers and the spin degrees of freedom. As found for $Ba(Fe_{1-x}Co_x)_2As_2$, a negative LMR is measured in LiFeAs. Although the value of the LMR coefficient is relatively large at low T and similar to that found in optimally doped Co–$BaFe_2As_2$, it decreases much more rapidly with increasing T and becomes nearly non-measurable above 50 K. This is quite in agreement with the rapid suppression of the NMR spin relaxation rate $1/T_1T$ [136].

By fitting the data in the same way as in the optimally and overdoped Co samples, we found that $\Delta\rho(H,T) \propto -H^2/T$ with a Curie–Weiss temperature $\theta \sim 0$, similarly to what is found for the 7.5%Co sample. So this can be taken as the sign that LiFeAs is located very near the boundary with the magnetic phase and that AF spin fluctuations could play a significant role in the superconductivity of this compound. This is in agreement with the INS observation of a peak in the imaginary part of the susceptibility at an incommensurate AF wave vector [137] despite the poor nesting between the electron and hole pockets observed by ARPES [127].

Different optical conductivity measurements have been reported in LiFeAs [138–140]. A Drude–Lorentz decomposition is used to fit the optical conductivity, in which the optical absorptions are described by separate contributions of the delocalised carriers at low frequencies (Drude peaks) and the excitations of the bound electrons at the high-frequency regions (Lorentz oscillators). One or two Drude peaks are usually used to fit the data. In Ref. [139], the analysis of the optical conductivity using one single Drude peak representative of the electron bands leads to a scattering rate that evolves linearly with temperature. The authors conclude that this linear behavior is compatible with spin fluctuations and supports the presence of a quantum critical point. However in a more recent study [140] where a coherent narrow Drude, a nearly incoherent broad Drude and series of Lorentz components are used, a T^2 dependence is reported for the scattering rate. Clearly it appears that the obtained results depend markedly on the parametrization of the normal state optical conductivity and that further investigations are needed to clarify this point. Let us recall that our transport analysis suggests that the effective mobilities of holes and electrons are rather similar, suggesting that the different bands should be also considered in the decomposition of the optical conductivity.

3.1.4. Effect of Co and Ni substitution on the Fe site

The substitution of Fe by small amounts of Co (or Ni) results in a monotonic lowering of T_c and of the superfluid stiffness [141]. Neither magnetic nor structural transitions have been detected in the temperature-doping (T–x) phase diagram of $LiFe_{1-x}Co_xAs$ (see Fig. 21a). T_c is lowered monotonically at a rate of 10 K per 0.1 electrons added per formula unit irrespective of whether the dopant is Co or Ni, and at higher doping levels superconductivity is completely suppressed. This indicates that the decrease in T_c is directly connected with the addition of electrons, as found in $Ba(Fe_{1-x}Co_x)_2As_2$. This is confirmed by ARPES measurements which show that the hole pockets shrink with Co doping while the electron pockets are enlarged [142].

The evolution of the resistivity curves at low T are reported in Fig. 21b for different Co contents. For each doping, $\rho(T)$ is fitted to a single power law $\rho(T) = \rho_0 + AT^n$, with the exponent n decreasing first from 2 in LiFeAs to 1.35 at $x \approx 0.12$, then increasing again up to 2 for $x = 0.4$ (see panel (f) in Fig. 21b). The authors conclude that it is the hallmark of a doping-induced FL–NFL–FL crossover in $LiFe_{1-x}Co_xAs$. However, let us notice that the Fermi surface topology evolves strongly with the introduction of Co substitution. In particular, the inner hole bands shrink and become electron-like for $x \geq 0.09$. On the other hand, determinations of the scattering rates from the momentum distribution curves indicate that the quasiparticle lifetime of the outer hole band made of the d_{xy} orbital is strongly reduced by the introduction of Co while those of the other bands are rather insensitive [142]. At last, it was shown that the bandwidth increases equally for all the bands, indicating the decrease of electronic correlations under Co doping [142]. It is clear that all these modifications of the electronic structure will have an important impact on the transport properties. It should be very interesting to perform Hall effect and magnetoresistance measurements, as done in pure LiFeAs [131] in order to be able to correlate the evolution of the transport properties with those of the electronic structure.

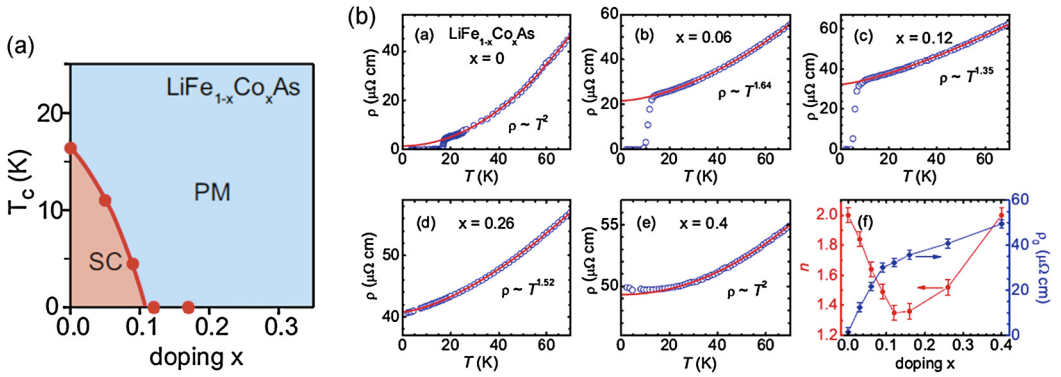

Fig. 21. (a) Phase diagram of $Li(Fe_{1-x}Co_x)As$, from [142]. Resistivity curves $\rho(T)$ (open blue circles) for a series of $Li(Fe_{1-x}Co_x)As$ for five selected Co contents. For each Co composition, $\rho(T)$ is fitted by a power law: $\rho(T) = \rho_0 + AT^n$ (solid red line). In the last panel, the exponent n and the residual resistivity ρ_0 are plotted versus the Co content x. From [140].

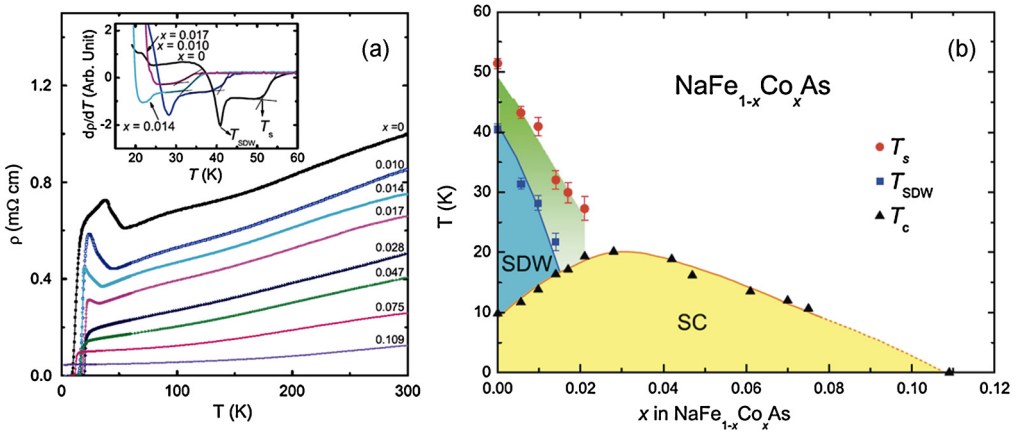

Fig. 22. (a) Resistivity as a function of temperature for selected $NaFe_{1-x}Co_xAs$ single crystals. The derivative of the resistivity for the underdoped crystals is reported in the inset, where the locations of the structural T_S and magnetic T_{SDW} transition temperatures are given. (b) Phase diagram of $NaFe_{1-x}Co_xAs$. T_S, T_{SDW}, and T_c are determined from the resistivity curves. From [146].

3.2. NaFeAs

Unlike LiFeAs, stoichiometric NaFeAs is superconducting with a $T_c \sim 10$ K and antiferromagnetic with a $T_N \sim 45$ K [143]. Replacement of Fe by Co suppresses both the structural and magnetic transition while enhances the superconducting transition temperature T_c. Optimal doping level is found for $x = 0.028$ and further doping of Co reduces T_c. It is found that the structural effects of Co and Ni doping are very similar, which demonstrates the dominant role of electron count in controlling the physics of these compounds [144]. The same conclusion is reached when comparing the effect of Co and Rh doping [145].

The resistivity curves for selected single crystals of $NaFe_{1-x}Co_xAs$ are displayed in Fig. 22a [146]. An upturn in resistivity is observed at low temperature for the underdoped crystals. As already reported in Fig. 1, the derivative of resistivity allows to figure out the temperatures corresponding to the structural and SDW transitions (T_S and T_{SDW}) and to determine the corresponding phase diagram (see Fig. 22b).

The evolution of the resistivity curves and the phase diagram of $NaFe_{1-x}Co_xAs$ display features very similar to those found in Co-doped 122 compounds. ARPES measurements show that the evolution of the electronic structure is very similar to what is found for Co substituted LiFeAs [147,142].

4. Conclusion

In this review we have reported representative transport studies for the 122 and 111 superconducting iron pnictides. It is clear that the key ingredient to understand these properties is the multi-band character of their electronic structure. This is a primordial difference with the cuprates. Even though multi-band materials were known and studied before as Sr_2RuO_4 for instance, it has been the discovery of the iron pnictides which initiated huge efforts to understand the incidence of their complex Fermi surfaces. This was possible thanks to the development of experimental methods as ARPES which was systematically used to map out the different electronic bands and theoretical calculations ([3] in this volume).

The complexity of their electronic structure implies that it is difficult to analyse transport properties without the help of further informations. The most illustrative example is certainly given by the study of LiFeAs, for which it has been shown that at least four different bands are necessary to account for the temperature evolution of the resistivity, Hall effect and orbital magnetoresistance [131]. Let us emphasize once again that this compound is particularly appropriate to make connections between surface and bulk properties since, owing to the absence of surface states, the surface properties are quite representative of those of the bulk. The rapid evolution of the electronic structure with electron or hole doping, as illustrated by ARPES [142] for $LiFe_{1-x}Co_xAs$ and $NaFe_{1-x}Co_xAs$ is probably the essential ingredient to understand the evolution of the transport properties. More experimental studies would be very interesting in these compounds to disentangle the contribution of the different bands to the transport properties.

One puzzling result of all these transport studies was to find that the scattering lifetimes of the holes are always (except for the hole doped 122 compound $Ba_{1-x}K_xFe_2As_2$) shorter than those of the electrons. To our knowledge, there is no theoretical consensus to explain this difference. However, this makes it possible to simplify the analyses of the transport properties as the contribution of some electronic (hole) bands can be neglected. This is why, starting from the simple two-band model to describe the transport properties of $Ba(Fe_{1-x}Co_x)_2As_2$ [6], we were able to show that a description in a single band framework was even appropriate for a range of T or x. This led us to conclude that the number of carriers increases with temperature, which was then confirmed by ARPES measurements [29]. This evidences that the very particular fermiology of these compounds results in very atypical properties, closer to those expected for semiconductor-like materials than for metals.

Recently detailed transport measurements were reported for the Iron chalcogenides due to advances in the high-quality single crystal growth [148–150]. The chalcogenide family exhibits the strongest electron correlations among the iron superconductors. The comparison of the evolution of the transport properties in iron pnictides and chalcogenides will certainly provide a new route to help elucidating these complex properties.

Acknowledgements

I would like to acknowledge my colleagues A. Forget and D. Colson for the very good iron-based single crystals which were used for the transport measurements. I thank H. Alloul for his fruitful collaboration about the interpretation of the transport data in $Ba(Fe_{1-x}Co_x)_2As_2$ and LiFeAs and his critical reading of this manuscript. Further I would like to acknowledge helpful discussions with P. Bonville, V. Brouet, J. Bobroff, Y. Gallais, Y. Laplace, M. Marsi and A. Olariu. This work has been performed within the “Triangle de la Physique” and was supported by the ANR grant “Pnictides”.

References

[1] J. Paglione, R.L. Greene, Nat. Phys. 6 (2010) 645.
[2] D.C. Johnston, Adv. Phys. 59 (2010) 803.
[3] A. van Roekeghem, P. Richard, H. Ding, S. Biermann, Spectral properties of transition metal pnictides and chalcogenides: angle-resolved photoemission spectroscopy and dynamical mean-field theory, C. R. Physique 17 (1–2) (2016) 140–163, this issue.
[4] I.I. Mazin, D.J. Singh, M.D. Johannes, M.H. Du, Phys. Rev. Lett. 101 (2008) 057003.
[5] P. Hirschfeld, Using gap symmetry and structure to reveal the pairing mechanism in Fe-based superconductors, C. R. Physique 17 (1–2) (2016) 197–231, this issue.
[6] F. Rullier-Albenque, D. Colson, A. Forget, H. Alloul, Phys. Rev. Lett. 103 (2009) 057001.
[7] A. Lankau, K. Koepernik, S. Borisenko, V. Zabolotnyy, B. Büchner, J. van den Brink, H. Eschrig, Phys. Rev. B 82 (2010) 184518.
[8] A. Leithe-Jasper, W. Schnelle, C. Geibel, H. Rosner, Phys. Rev. Lett. 101 (2008) 207004.
[9] A.S. Sefat, R. Jin, M.A. McGuire, B.C. Sales, D.J. Singh, D. Mandrus, Phys. Rev. Lett. 101 (2008) 117004.
[10] N. Ni, M.E. Tillman, J.-Q. Yan, A. Kracher, S.T. Hannahs, S.L. Bud'ko, P.C. Canfield, Phys. Rev. B 78 (2008) 214515.
[11] S. Sharma, A. Bharathi, S. Chandra, R. Reddy, S. Paulraj, A. Satya, V. Sastry, A. Gupta, C. Sundar, Phys. Rev. B 81 (2010) 174512.
[12] W. Schnelle, A. Leithe-Jasper, R. Gumeniuk, U. Burkhardt, D. Kasinathan, H. Rosner, Phys. Rev. B 79 (2009) 214516.
[13] M. Rotter, M. Tegel, D. Johrendt, Phys. Rev. Lett. 101 (2008) 107006.
[14] Zhi Ren, Qian Tao, Shuai Jiang, Chunmu Feng, Cao Wang, Jianhui Dai, Guanghan Cao, Zhu'an Xu, Phys. Rev. Lett. 102 (2009) 137002.
[15] Shuai Jiang, Hui Xing, Guofang Xuan, Cao Wang, Zhi Ren, Chunmu Feng, Jianhui Dai, Zhu'an Xu, Guanghan Cao, J. Phys. Condens. Matter 21 (2009) 382203.
[16] S. Kasahara, T. Shibauchi, K. Hashimoto, K. Ikada, S. Tonegawa, R. Okazaki, H. Shishido, H. Ikeda, H. Takeya, K. Hirata, T. Terashima, Y. Matsuda, Phys. Rev. B 81 (2010) 184519.
[17] S.R. Saha, N.P. Butch, K. Kirshenbaum, Johnpierre Paglione, P.Y. Zavali, Phys. Rev. Lett. 103 (2009) 037005.
[18] A. Martinelli, F. Bernardini, S. Massida, The phase diagrams of iron-based superconductors: theory and experiments, C. R. Physique 17 (1–2) (2016) 5–35, this issue.
[19] Krzysztof Gofryk, Minghu Pan, Claudia Cantoni, Bayrammurad Saparov, Jonathan E. Mitchell, Athena S. Sefat, Phys. Rev. Lett. 112 (2014) 047005.
[20] A. Olariu, F. Rullier-Albenque, D. Colson, A. Forget, Phys. Rev. B 83 (2011) 054518.
[21] Fanlong Ning, Kanagasingham Ahilan, Takashi Imai, Athena S. Sefat, Ronying Jin, Michael A. McGuire, Brian C. Sales, David Mandrus, J. Phys. Soc. Jpn. 78 (2009) 013711.
[22] V. Brouet, M. Marsi, B. Mansart, A. Nicolaou, A. Taleb-Ibrahimi, P. Le Fèvre, F. Bertran, F. Rullier-Albenque, A. Forget, D. Colson, Phys. Rev. B 80 (2009) 165115.
[23] Y. Sekiba, T. Sato, K. Nakayama, K. Terashima, P. Richard, J.H. Bowen, H. Ding, Y.-M. Xu, L.J. Li, G.H. Cao, Z.-A. Xu, T. Takahashi, New J. Phys. 11 (2009) 025020.
[24] S. Ideta, T. Yoshida, I. Nishi, A. Fujimori, Y. Kotani, K. Ono, Y. Nakashima, S. Yamaichi, T. Sasagawa, M. Nakajima, K. Kihou, Y. Tomioka, C.H. Lee, A. Iyo, H. Eisaki, T. Ito, S. Uchida, R. Arita, Phys. Rev. Lett. 110 (2013) 107007.
[25] H. Wadati, I. Elfimov, G.A. Sawatzky, Phys. Rev. Lett. 105 (2010) 157004.

[26] P.C. Canfield, S.L. Bud'ko, Annu. Rev. Condens. Matter Phys. 1 (2010) 27–50.
[27] Qimiao Si, Elihu Abrahams, Phys. Rev. Lett. 101 (2008) 076401.
[28] K. Haule, G. Kottliar, New J. Phys. 11 (2009) 025021.
[29] V. Brouet, P.-H. Lin, Y. Texier, J. Bobroff, A. Taleb-Ibrahimi, P. Le Févre, F. Bertran, M. Casula, P. Werner, S. Biermann, F. Rullier-Albenque, A. Forget, D. Colson, Phys. Rev. Lett. 110 (2013) 167002.
[30] Y. Wang, Maria N. Gastiasoro, Brian M. Andersen, M. Tomić, Harald O. Jeschke, Roser Valentí, Indranil Paul, P.J. Hirschfeld, Phys. Rev. Lett. 114 (2015) 097003.
[31] F. Rullier-Albenque, D. Colson, A. Forget, unpublished results.
[32] Lei Fang, Huiqian Luo, Peng Cheng, Zhaosheng Wang, Ying Jia, Gang Mu, Bing Shen, I.I. Mazin, Lei Shan, Cong Ren, Hai-Hu Wen, Phys. Rev. B 80 (2009) 140508(R).
[33] R.S. Dhaka, S.E. Hahn, E. Razzoli, R. Jiang, M. Shi, B.N. Harmon, A. Thaler, S.L. Bud'ko, P.C. Canfield, A. Kaminski, Phys. Rev. Lett. 110 (2013) 067002.
[34] B. Muschler, W. Prestel, R. Hackl, T.P. Devereaux, J.G. Analytis, J.-H. Chu, I.R. Fisher, Phys. Rev. B 80 (2009) 180510(R).
[35] E.G. Maksimov, A.E. Karakozov, B.P. Gorshunov, A.S. Prokhorov, A.A. Voronkov, E.S. Zhukova, V.S. Nozdrin, S.S. Zhukov, D. Wu, M. Dressel, S. Haindl, K. Iida, B. Holzapfel, Phys. Rev. B 83 (2011) 140502(R).
[36] A.F. Kemper, M.M. Korshunov, T.P. Devereaux, J.N. Fry, H.-P. Cheng, P.J. Hirschfeld, Phys. Rev. B 83 (2011) 184516.
[37] Maxim Breitkreiz, P.M.R. Brydon, Carsten Timm, Phys. Rev. B 89 (2014) 245016.
[38] L. Benfatto, E. Cappelluti, Phys. Rev. B 83 (2011) 104516.
[39] Melissa Gooch, Bing Lv, Bernd Lorenz, Arnold M. Guloy, Ching-Wu Chu, Phys. Rev. B 79 (2009) 104504.
[40] Nicolas Doiron-Leyraud, Pascale Auban-Senzier, Samuel René de Cotret, Claude Bourbonnais, Denis Jérome, Klaus Bechgaard, Louis Taillefer, Phys. Rev. B 80 (2009) 214531.
[41] N.W. Ashcroft, N.D. Mermin, Solid State Physics, Saunders College Publishing, Philadelphia, 1976.
[42] L. Fanfarillo, E. Cappelluti, C. Castellani, L. Benfatto, Phys. Rev. Lett. 109 (2012) 096402.
[43] F.L. Ning, K. Ahilan, T. Imai, A.S. Sefat, M.A. McGuire, B.C. Sales, D. Mandrus, P. Cheng, B. Shen, H.H. Wen, Phys. Rev. Lett. 104 (2010) 037001.
[44] R. Zhou, Z. Li, J. Yang, D.L. Sun, C.T. Lin, Guo-qing Zheng, Nat. Commun. 4 (2013) 2265.
[45] N. Barišić, D. Wu, M. Dressel, L.J. Li, G.H. Cao, Z.A. Xu, Phys. Rev. B 82 (2010) 054518.
[46] F. Rullier-Albenque, D. Colson, A. Forget, Phys. Rev. B 88 (2013) 045105.
[47] T. Moriya, Spin Fluctuations in Itinerant Electron Magnetism, Springer Series in Solid State Sciences, vol. 56, Springer-Verlag, 1985.
[48] K. Usami, T. Moriya, J. Phys. Soc. Jpn. 44 (1978) 122.
[49] D.S. Inosov, J.T. Park, P. Bourges, D.L. Sun, Y. Sidis, A. Schneidewind, K. Hradil, D. Haug, C.T. Lin, B. Keimer, V. Hinkov, Nat. Phys. 6 (2010) 178.
[50] L. de'Medici, S.R. Hassan, M. Capone, J. Supercond. Nov. Magn. 22 (2009) 535.
[51] Z.P. Yin, K. Haule, G. Kotliar, Nat. Mater. 10 (2011) 932–935.
[52] L. de'Medici, G. Giovannetti, M. Capone, arXiv:1212.3966, unpublished.
[53] I. Paul, G. Kottliar, Phys. Rev. B 64 (2001) 184414.
[54] S. Arsenijević, H. Hodovanets, R. Gaál, L. Forró, S.L. Bud'ko, P.C. Canfield, Phys. Rev. B 87 (2013) 224508.
[55] D. Hsieh, Y. Xia, L. Wray, D. Qian, K.K. Gomes, A. Yazdani, G.F. Chen, J.L. Luo, N.L. Wang, M.Z. Hasan, arXiv:0812.2289, 2008, unpublished.
[56] Chang Liu, Takeshi Kondo, Rafael M. Fernandes, Ari D. Palczewski, Eun Deok Mun, Ni Ni, Alexander N. Thaler, Aaron Bostwick, Eli Rotenberg, Jörg Schmalian, Sergey L. Bud'ko, Paul C. Canfield, Adam Kaminski, Nat. Phys. 6 (2010) 419.
[57] P. Richard, K. Nakayama, T. Sato, M. Neupane, Y.-M. Xu, J.H. Bowen, G.F. Chen, J.L. Luo, N.L. Wang, X. Dai, Z. Fang, H. Ding, T. Takahashi, Phys. Rev. Lett. 104 (2010) 137001.
[58] Yeongkwan Kim, Hyungju Oh, Chul Kim, Dongjoon Song, Wonsig Jung, Beomyoung Kim, Hyoung Joon Choi, Changyoung Kim, Bumsung Lee, Seunghyun Khim, Hyungjoon Kim, Keehoon Kim, Jongbeom Hong, Yongseung Kwon, Phys. Rev. B 83 (2011) 064509.
[59] M. Fuglsang Jensen, V. Brouet, E. Papalazarou, A. Nicolaou, A. Taleb-Ibrahimi, P. Le Fèvre, F. Bertran, A. Forget, D. Colson, Phys. Rev. B 84 (2011) 014509.
[60] Suchitra E. Sebastian, J. Gillett, N. Harrison, P.H.C. Lau, D.J. Singh, C.H. Mielke, G.G. Lonzarich, J. Phys. Condens. Matter 20 (2008) 422203.
[61] James G. Analytis, Ross D. McDonald, Jiun-Haw Chu, Scott C. Riggs, Alimamy F. Bangura, Chris Kucharczyk, Michelle Johannes, I.R. Fisher, Phys. Rev. B 80 (2009) 064507.
[62] Taichi Terashima, Nobuyuki Kurita, Megumi Tomita, Kunihiro Kihou, Chul-Ho Lee, Yasuhide Tomioka, Toshimitsu Ito, Akira Iyo, Hiroshi Eisaki, Tian Liang, Masamichi Nakajima, Shigeyuki Ishida, Shin-ichi Uchida, Hisatomo Harima, Shinya Uji, Phys. Rev. Lett. 107 (2011) 176402.
[63] K.K. Huynh, Y. Tanabe, K. Tanigaki, Phys. Rev. Lett. 106 (2011) 217004.
[64] H.H. Kuo, J.H. Chu, S.C. Riggs, L. Yu, P.L. McMahon, K. De Greve, Y. Yamamoto, J.G. Analytis, I.R. Fisher, Phys. Rev. B 84 (2011) 054540.
[65] S. Ishida, T. Liang, M. Nakajima, K. Kihou, C.H. Lee, A. Iyo, H. Eisaki, T. Kakeshita, T. Kida, M. Hagiwara, Y. Tomioka, T. Ito, S. Uchida, Phys. Rev. B 84 (2011) 184514.
[66] C.R. Rotundu, B. Freelon, T.R. Forrest, S.D. Wilson, P.N. Valdivia, G. Pinuellas, A. Kim, J.-W. Kim, Z. Islam, E. Bourret-Courchesne, N.E. Phillips, R.J. Birgeneau, Phys. Rev. B 82 (2010) 144525.
[67] H.Q. Yuan, L. Jiao, F.F. Balakirev, J. Singleton, C. Setty, J.P. Hu, T. Shang, L.J. Li, G.H. Cao, Z.A. Xu, B. Shen, H.H. Wen, arXiv:1102.5476, 2011, unpublished.
[68] Y.-X. Yang, Y. Gallais, F. Rullier-Albenque, M.-A. Méasson, M. Cazayous, A. Sacuto, J. Shi, D. Colson, A. Forget, Phys. Rev. B 89 (2014) 125130.
[69] E.D. Mun, S.L. Bud'ko, N. Ni, A.N. Thaler, P.C. Canfield, Phys. Rev. B 80 (2009) 054517.
[70] H. Hodovanets, A. Thaler, E. Mun, N. Ni, S.L. Bud'ko, P.C. Canfield, Philos. Mag. 93 (6) (2012) 661.
[71] Jiun-Haw Chu, James G. Analytis, Kristiaan De Greve, Peter L. McMahon, Zahirul Islam, Yoshihisa Yamamoto, Ian R. Fisher, Science 329 (2010) 824.
[72] Hsueh-Hui Kuo, Ian R. Fisher, Phys. Rev. Lett. 112 (2014) 227001.
[73] S. Ishida, M. Nakajima, T. Liang, K. Kihou, C.H. Lee, A. Iyo, H. Eisaki, T. Kakeshita, Y. Tomioka, T. Ito, S. Uchida, Phys. Rev. Lett. 110 (2013) 207001.
[74] V. Brouet, F. Rullier-Albenque, M. Marsi, B. Mansart, M. Aichhorn, S. Biermann, J. Faure, L. Perfetti, A. Taleb-Ibrahimi, P. Le Fèvre, F. Bertran, A. Forget, D. Colson, Phys. Rev. Lett. 105 (2010) 087001.
[75] N. Xu, T. Qian, P. Richard, Y.-B. Shi, X.-P. Wang, P. Zhang, Y.-B. Huang, Y.-M. Xu, H. Miao, G. Xu, G.-F. Xuan, W.-H. Jiao, Z.-A. Xu, G.-H. Cao, H. Ding, Phys. Rev. B 86 (2012) 064505.
[76] F. Rullier-Albenque, D. Colson, A. Forget, P. Thuéry, S. Poissonnet, Phys. Rev. B 81 (2010) 224503.
[77] A. Thaler, N. Ni, A. Kracher, J.Q. Yan, S.L. Bud'ko, P.C. Canfield, Phys. Rev. B 82 (2010) 014534.
[78] Y. Laplace, J. Bobroff, V. Brouet, G. Collin, F. Rullier-Albenque, D. Colson, A. Forget, Phys. Rev. B 86 (2012) 020510.
[79] Y. Laplace, J. Bobroff, F. Rullier-Albenque, D. Colson, A. Forget, Phys. Rev. B 80 (2009) 140501(R).
[80] M.J. Eom, S.W. Na, C. Hoch, R.K. Kremer, J.S. Kim, Phys. Rev. B 85 (2012) 024536.
[81] H. Hodovanets, E.D. Mun, A. Thaler, S.L. Bud'ko, P.C. Canfield, Phys. Rev. B 83 (2011) 094508.
[82] F. Rullier-Albenque, D. Colson, A. Forget, unpublished results.
[83] Limin Wang, Tom Berlijn, Yan Wang, Chia-Hui Lin, P.J. Hirschfeld, Wei Ku, Phys. Rev. Lett. 110 (2013) 037001.
[84] H. Shishido, A.F. Bangura, A.I. Coldea, S. Tonegawa, K. Hashimoto, S. Kasahara, P.M.C. Rourke, H. Ikeda, T. Terashima, R. Settai, Y. Ōnuki, D. Vignolles, C. Proust, B. Vignolle, A. McCollam, Y. Matsuda, T. Shibauchi, A. Carrington, Phys. Rev. Lett. 104 (2010) 057008.

[85] T. Shibauchi, A. Carrington, Y. Matsuda, Annu. Rev. Condens. Matter Phys. 5 (2014) 113–135.
[86] T. Yoshida, I. Nishi, S. Ideta, A. Fujimori, M. Kubota, K. Ono, S. Kasahara, T. Shibauchi, T. Terashima, Y. Matsuda, H. Ikeda, R. Arita, Phys. Rev. Lett. 106 (2011) 117001.
[87] James G. Analytis, H.-H. Kuo, Ross D. McDonald, Mark Wartenbe, P.M.C. Rourke, N.E. Hussey, I.R. Fisher, Nat. Phys. 10 (2014) 194.
[88] Y. Nakai, T. Iye, S. Kitagawa, K. Ishida, H. Ikeda, S. Kasahara, H. Shishido, T. Shibauchi, Y. Matsuda, T. Terashima, Phys. Rev. Lett. 105 (2010) 107003.
[89] K. Hashimoto, K. Cho, T. Shibauchi, S. Kasahara, Y. Mizukami, R. Katsumata, Y. Tsuruhara, T. Terashima, H. Ikeda, M.A. Tanatar, H. Kitano, N. Salovich, R.W. Giannetta, P. Walmsley, A. Carrington, R. Prozorov, Y. Matsuda, Science 336 (2012) 1554.
[90] P. Walmsley, C. Putzke, L. Malone, I. Guillamón, D. Vignolles, C. Proust, S. Badoux, A.I. Coldea, M.D. Watson, S. Kasahara, Y. Mizukami, T. Shibauchi, Y. Matsuda, A. Carrington, Phys. Rev. Lett. 110 (2013) 257002.
[91] H.S. Jeevan, Deepa Kasinathan, Helge Rosner, Philipp Gegenwart, Phys. Rev. B 83 (2011) 054511.
[92] I. Nowik, I. Felner, Z. Ren, G.H. Cao, Z.A. Xu, J. Phys. Condens. Matter 23 (2011) 065701.
[93] S. Zapf, H.S. Jeevan, T. Ivek, F. Pfister, F. Klingert, S. Jiang, D. Wu, P. Gegenwart, R.K. Kremer, M. Dressel, Phys. Rev. Lett. 110 (2013) 237002.
[94] S. Zapf, D. Neubauer, K.W. Post, A. Kadau, J. Merz, C. Clauss, A. Löhle, H.S. Jeevan, P. Gegenwart, D.N. Basov, M. Dressel, Electronic scattering effects in europium-based iron pnictides, C. R. Physique 17 (1–2) (2016) 188–196, this issue.
[95] J.P. Clancy, B.D. Gaulin, A.S. Sefat, Phys. Rev. B 85 (2012) 054115.
[96] A. Thaler, H. Hodovanets, M.S. Torikachvili, S. Ran, A. Kracher, W. Straszheim, J.Q. Yan, E. Mun, P.C. Canfield, Phys. Rev. B 84 (2011) 144528.
[97] Y. Texier, Y. Laplace, P. Mendels, J.T. Park, G. Friemel, D.L. Sun, D.S. Inosov, C.T. Lin, J. Bobroff, Europhys. Lett. 99 (2012) 17002.
[98] H. Suzuki, T. Yoshida, S. Ideta, G. Shibata, K. Ishigami, T. Kadono, A. Fujimori, M. Hashimoto, D.H. Lu, Z.-X. Shen, K. Ono, E. Sakai, H. Kumigashira, M. Matsuo, T. Sasagawa, Phys. Rev. B 88 (2013) 100501(R).
[99] T. Urata, Y. Tanabe, K.K. Huynh, H. Oguro, K. Watanabe, S. Heguri, K. Tanigaki, Phys. Rev. B 89 (2014) 024503.
[100] T. Urata, Y. Tanabe, K.K. Huynh, S. Heguri, H. Oguro, K. Watanabe, K. Tanigaki, Phys. Rev. B 91 (2015) 174508.
[101] B. Shen, H. Yang, Z.-S. Wang, F. Han, B. Zeng, L. Shan, C. Ren, H.-H. Wen, Phys. Rev. B 84 (2011) 184512.
[102] H. Chen, Y. Ren, Y. Qiu, W. Bao, R.H. Liu, G. Wu, T. Wu, Y.L. Xie, X.F. Wang, Q. Huang, X.H. Chen, Europhys. Lett. 85 (2009) 17006.
[103] Kenya Ohgushi, Yoko Kiuchi, Phys. Rev. B 85 (2012) 064522.
[104] Y. Liu, M.A. Tanatar, W.E. Straszheim, B. Jensen, K.W. Dennis, R.W. McCallum, V.G. Kogan, R. Prozorov, T.A. Lograsso, Phys. Rev. B 89 (2014) 134504.
[105] D. Wu, N. Bariˇsi´c, P. Kallina, A. Faridian, B. Gorshunov, N. Drichko, L.J. Li, X. Lin, G.H. Cao, Z.A. Xu, N.L. Wang, M. Dressel, Phys. Rev. B 81 (2010) 100512.
[106] A.A. Golubov, O.V. Dolgov, A.V. Boris, A. Charnukha, D.L. Sun, C.T. Lin, A.F. Shevchun, A.V. Korobenko, M.R. Trunin, V.N. Zverev, JETP Lett. 94 (2011) 333.
[107] Y.M. Dai, B. Xu, B. Shen, H. Xiao, H.H. Wen, X.G. Qiu, C.C. Homes, R.P.S.M. Lobo, Phys. Rev. Lett. 111 (2013) 117001.
[108] Kevin Kirshenbaum, S.R. Saha, S. Ziemak, T. Drye, J. Paglione, Phys. Rev. B 86 (2012) 140505(R).
[109] Veronika Zinth, Til Dellmann, Hans-Henning Klauss, Dirk Johrendt, Angew. Chem., Int. Ed. Engl. 50 (2011) 7919.
[110] Takayoshi Katase, Soshi Iimura, Hidenori Hiramatsu, Toshio Kamiya, Hideo Hosono, Phys. Rev. B 85 (2012) 140516(R).
[111] E.C. Blomberg, M.A. Tanatar, R.M. Fernandes, I.I. Mazin, Bing Shen, Hai-Hu Wen, M.D. Johannes, J. Schmalian, R. Prozorov, Nat. Commun. 4 (2013) 1914.
[112] Tatsuya Kobayashi, Kiyohisa Tanaka, Shigeki Miyasaka, Setsuko Tajima, J. Phys. Soc. Jpn. 84 (2015) 094707.
[113] M.P. Allan, T.-M. Chuang, F. Massee, Yang Xie, Ni Ni, S.L. Bud'ko, G.S. Boebinger, Q. Wang, D.S. Dessau, P.C. Canfield, M.S. Golden, J.C. Davis, Nat. Phys. 9 (2013) 220.
[114] Maria N. Gastiasoro, I. Paul, Y. Wang, P.J. Hirschfeld, Brian M. Andersen, Phys. Rev. Lett. 113 (2014) 127001.
[115] Rafael M. Fernandes, Elihu Abrahams, Jörg Schmalian, Phys. Rev. Lett. 107 (2011) 217002.
[116] Anna E. Böhmer, Christoph Meingast, Electronic nematic susceptibility of iron-based superconductors, C. R. Physique 17 (1–2) (2016) 90–112, this issue.
[117] Y. Gallais, I. Paul, Charge nematicity and electronic Raman scattering in iron-based superconductors, C. R. Physique 17 (1–2) (2016) 113–139, this issue.
[118] M.A. Tanatar, N. Ni, A. Thaler, S.L. Bud'ko, P.C. Canfield, R. Prozorov, Phys. Rev. B 82 (2010) 134528.
[119] M.A. Tanatar, N. Ni, A. Thaler, S.L. Bud'ko, P.C. Canfield, R. Prozorov, Phys. Rev. B 84 (2011) 014519.
[120] M.A. Tanatar, W.E. Straszheim, Hyunsoo Kim, J. Murphy, N. Spyrison, E.C. Blomberg, K. Cho, J.-Ph. Reid, Bing Shen, Louis Taillefer, Hai-Hu Wen, R. Prozorov, Phys. Rev. B 89 (2014) 144514.
[121] M.A. Tanatar, K. Hashimoto, S. Kasahara, T. Shibauchi, Y. Matsuda, R. Prozorov, Phys. Rev. B 87 (2013) 104506.
[122] M.A. Tanatar, M.S. Torikachvili, A. Thaler, S.L. Bud'ko, P.C. Canfield, R. Prozorov, Phys. Rev. B 90 (2014) 104518.
[123] S.J. Moon, A.A. Schafgans, S. Kasahara, T. Shibauchi, T. Terashima, Y. Matsuda, M.A. Tanatar, R. Prozorov, A. Thaler, P.C. Canfield, A.S. Sefat, D. Mandrus, D.N. Basov, Phys. Rev. Lett. 109 (2012) 027006.
[124] S.J. Moon, A.A. Schafgans, M.A. Tanatar, R. Prozorov, A. Thaler, P.C. Canfield, A.S. Sefat, D. Mandrus, D.N. Basov, Phys. Rev. Lett. 110 (2013) 097003.
[125] Y.M. Dai, B. Xu, B. Shen, H.H. Wen, J.P. Hu, X.G. Qiu, R.P.S.M. Lobo, Phys. Rev. B 86 (2012) 100501(R).
[126] A.W. Tyler, A.P. Mackenzie, S. NishiZaki, Y. Maeno, Phys. Rev. B 58 (1998) 10107(R).
[127] S.V. Borisenko, V.B. Zabolotnyy, D.V. Evtushinsky, T.K. Kim, I.V. Morozov, A.N. Yaresko, A.A. Kordyuk, G. Behr, A. Vasiliev, R. Follath, B. Büchner, Phys. Rev. Lett. 105 (2010) 067002.
[128] K. Umezawa, Y. Li, H. Miao, K. Nakayama, Z.-H. Liu, P. Richard, T. Sato, J.B. He, D.-M. Wang, G.F. Chen, H. Ding, T. Takahashi, S.-C. Wang, Phys. Rev. Lett. 108 (2012) 037002.
[129] O. Heyer, T. Lorenz, V.B. Zabolotnyy, D.V. Evtushinsky, S.V. Borisenko, I. Morozov, L. Harnagea, S. Wurmehl, C. Hess, B. Büchner, Phys. Rev. B 84 (2011) 064512.
[130] S. Kasahara, K. Hashimoto, H. Ikeda, T. Terashima, Y. Matsuda, T. Shibauchi, Phys. Rev. B 85 (2012) 060503.
[131] F. Rullier-Albenque, D. Colson, A. Forget, H. Alloul, Phys. Rev. Lett. 109 (2012) 187005, *ibid.* Phys. Rev. Lett. 113 (2014) 209901.
[132] J. Ferber, K. Foyevtsova, R. Valenti, H.O. Jeschke, Phys. Rev. B 85 (2012) 094505.
[133] S.V. Borisenko, D.V. Evtushinsky, I. Morozov, S. Wurmehl, B. Büchner, A.N. Yaresko, T.K. Kim, M. Hoesch, T. Wolf, N.D. Zhigadlo, arXiv:1409.8669, 2014, unpublished.
[134] C. Putzke, A.I. Coldea, I. Guillamon, D. Vignolles, A. McCollam, D. LeBoeuf, M.D. Watson, I.I. Mazin, S. Kasahara, T. Terashima, T. Shibauchi, Y. Matsuda, A. Carrington, Phys. Rev. Lett. 108 (2012) 047002.
[135] A.A. Kordyuk, V.B. Zabolotnyy, D.V. Evtushinshky, T.K. Kim, L.V. Morozov, M.L. Kulić, R. Follath, G. Behr, B. Büchner, S.V. Borisenko, Phys. Rev. B 83 (2011) 134513.
[136] L. Ma, J. Zhang, G.F. Chen, W. Yu, Phys. Rev. B 82 (2010) 180501(R).
[137] N. Qureshi, P. Steffens, Y. Drees, A.C. Komarek, D. Lamago, Y. Sidis, L. Harnagea, H.-J. Grafe, S. Wurmehl, B. Büchner, M. Braden, Phys. Rev. Lett. 108 (2012) 117001.
[138] Byeong Hun Min, Jong Beom Hong, Jae Hyun Yun, Takuya Iizuka, Shin-ichi Kimura, Yunkyu Bang, Yong Seung Kwon, New J. Phys. 15 (2013) 073029.

[139] R.P.S.M. Lobo, G. Chanda, A.V. Pronin, J. Wosnitza, S. Kasahara, T. Shibauchi, Y. Matsuda, Phys. Rev. B 91 (2015) 174509.
[140] Y.M. Dai, H. Miao, L.Y. Xing, X.C. Wang, P.S. Wang, H. Xiao, T. Qian, P. Richard, X.G. Qiu, W. Yu, C.Q. Jin, Z. Wang, P.D. Johnson, C.C. Homes, H. Ding, Phys. Rev. X 5 (2015) 031035.
[141] M.J. Pitcher, T. Lancaster, J.D. Wright, I. Franke, A.J. Steele, P.J. Baker, F.L. Pratt, W.T. Thomas, D.R. Parker, S.J. Blundell, S.J. Clarke, J. Am. Chem. Soc. 132 (2010) 10467.
[142] Z.R. Ye, Y. Zhang, M. Xu, Q.Q. Ge, Q. Fan, F. Chen, J. Jiang, P.S. Wang, J. Dai, W. Yu, B.P. Xie, D.L. Feng, arXiv:1303.0682, 2013, unpublished.
[143] Dinah R. Parker, Michael J. Pitcher, Peter J. Baker, Isabel Franke, Tom Lancaster, Stephen J. Blundell, Simon J. Clarke, Chem. Commun. (2009) 2189.
[144] Dinah R. Parker, Matthew J.P. Smith, Tom Lancaster, Andrew J. Steele, Isabel Franke, Peter J. Baker, Francis L. Pratt, Michael J. Pitcher, Stephen J. Blundell, Simon J. Clarke, Phys. Rev. Lett. 104 (2010) 057007.
[145] Frank Steckel, Maria Roslova, Robert Beck, Igor Morozov, Saicharan Aswartham, Daniil Evtushinsky, Christian G.F. Blum, Mahmoud Abdel-Hafiez, Dirk Bombor, Janek Maletz, Sergey Borisenko, Andrei V. Shevelkov, Anja U.B. Wolter, Christian Hess, Sabine Wurmehl, Bernd Büchner, Phys. Rev. B 91 (2015) 184516.
[146] A.F. Wang, X.G. Luo, Y.J. Yan, J.J. Ying, Z.J. Xiang, G.J. Ye, P. Cheng, Z.Y. Li, W.J. Hu, X.H. Chen, Phys. Rev. B 85 (2012) 224521.
[147] S.T. Cui, S.Y. Zhu, A.F. Wang, S. Kong, S.L. Ju, X.G. Luo, X.H. Chen, G.B. Zhang, Z. Sun, Phys. Rev. B 86 (2012) 155143.
[148] K.K. Huynh, Y. Tanabe, T. Urata, H. Oguro, S. Heguri, K. Watanabe, K. Tanigaki, Phys. Rev. B 90 (2014) 144516.
[149] V.L. Bezusyy, D.J. Gawryluk, A. Malinowski, Marta Z. Cieplak, Phys. Rev. B 91 (2015) 100502(R).
[150] M.D. Watson, T. Yamashita, S. Kasahara, W. Knafo, M. Nardone, J. Beard, F. Hardy, A. McCollam, A. Narayanan, S.F. Blake, T. Wolf, A.A. Haghighirad, C. Meingast, A.J. Schofield, H. von Lohneysen, Y. Matsuda, A.I. Coldea, T. Shibauchi, arXiv:1502.02922, 2015, unpublished.